Spring 2012

Design of a controlled environment agricultural plant inspection robot

Howard Chen
University of Iowa

DESIGN OF A CONTROLLED ENVIRONMENT AGRICULTURAL PLANT INSPECTION ROBOT

by

Howard Chen

A thesis submitted in partial fulfillment
of the requirements for the
Master of Science degree in Industrial Engineering
in the Graduate College of
The University of Iowa

May 2012

Thesis Supervisor: Associate Professor Geb Thomas

Graduate College
The University of Iowa
Iowa City, Iowa

CERTIFICATE OF APPROVAL

_____

MASTER'S THESIS

_____

This is to certify that the Master's thesis of

Howard Chen

has been approved by the Examining Committee
for the thesis requirement for the Master of Science
degree in Industrial Engineering at the
May 2012 graduation

Thesis Committee: _____
Geb Thomas, Thesis Supervisor

_____
Ibrahim Ozbolat

_____
Albert Ratner

ACKNOWLEDGEMENTS

I would like to give my sincerest thanks to my advisor; Prof. Geb Thomas, who took me on early in my sophomore year as an undergraduate, a point in time where very few other professors would see value in a student. Throughout my time here at Iowa, he gave me opportunities that I have never dreamed of, exposed me to subject matters that I have never heard of, challenged and changed my way of thinking, showed me my strengths and worked on my weaknesses and, most importantly, taught me how to think like an engineer. Although his efforts and time that he invested in me could never be repaid in full, without him, I would definitely have been a lost soul working in a cubicle farm.

I would like to thank Prof. Albert Ratner and Ibrahim Ozbolat for being on my thesis committee. I would like to thank Prof. Ratner additionally for mentoring me for my undergraduate senior design project, which turned from a joke to a project worthy to be presented to the President of the university. I would like to thank Prof. Ozbolat additionally for taking me on as one of his first doctoral candidates.

Additionally, I would like to thank Brian Johns and Matias Perret for teaching me the various skills required to be a semi-competent machinist.

Last but certainly not the least, I would like to thank my family for their constant and unconditional support of the various decisions that I have made in my life, including the pursuit of graduate studies.

ABSTRACT

Without an increase in cropland, agricultural efficiency must be tripled in the next 50 years to sustain the increased demand for food. Controlled environment agriculture (CEA) systems are likely to play an important role in the increase of agricultural efficiency. CEA systems, however, require constant observation because decisions must be quickly made when plants show signs of stress. A visual inspection system that uses a robotic camera system would permit visual access to inaccessible plants in a large hydroponics operation or allows an observer to remotely inspect plants for multiple small or remote CEA operations, whereas a dedicated CEA specialist would be beneficial but impractical under present conditions.

This thesis presents a theoretical design for a plant inspection robot. The design parameters, design process, and the system specification necessary to satisfy the design constraints were examined for this system. The design analysis revealed that the major components of the plant inspection robot must be designed sequentially, starting with the imaging system. The imaging system design revealed that the system parameters were governed by illumination, shape and size of the object, and the desired detail. The motion system design was governed by velocity, acceleration, work area, and accuracy. An example design for a system used for visual inspection of 289 romaine lettuce plants was presented. This design was shown to be feasible from the theoretical perspective and could be built from commercially-available components, reducing development time and cost.

TABLE OF CONTENTS

LIST OF TABLES

LIST OF FIGURES

CHAPTER 1

INTRODUCTION

1.1 Background

In order to meet the rising demand for food, agricultural efficiency must be tripled in the next 50 years to sustain the increased demand for food without an increase in cropland. The increased demand for food is caused by human population growth, which is projected to reach 9 billion by the middle of this century, and compounded by the increased consumption of meat and dairy products, which requires three to five times as much farming resources per calorie to produce as rice or wheat (Avery, 2007).

Controlled environment agriculture (CEA) systems are likely to play an important role in increases agricultural efficiency. CEA systems grow crops in an enclosed environment in which all aspects of the natural environment, including air and root temperatures, light, water, humidity, carbon dioxide, and plant nutrition, are precisely controlled. The tight control of these parameters enables a 15-50% savings in for energy, water, chemical, and pesticide applications, while producing plants with higher consistency and overall quality (Jensen, 2002). A CEA system is able to produce an annual expected yield three to four times larger than traditional agricultural methods because of closer plant spacing, faster maturing time, and year round production (Harris, 1992).

Hydroponics, a method used to grow plants in nutrient solutions instead of soil, is frequently used in CEA systems to further increase agricultural efficiency. Hydroponic systems provide crops with nutrition dissolved in the water, which is absorbed at a faster rate compared to soil and enables crop nutrition to be precisely controlled (Gorbe & Calatayud, 2010). In a floating hydroponic system, which is often used for growing lettuces, the plants are grown on floating rafts in a large pool of fertilized water. Such

systems are capable of producing 10 times the annual yield compared to traditional open-field lettuce productions (Story, Kacira, Kubota, Akoglu, & An, 2010).

CEA systems require constant monitoring because quick action is often required when plants show signs of stress. Plant nutrition in hydroponic systems can change over time, causing even well-designed crop production systems to have problems with excess and deficiencies (Alaya-Silva & Beyl, 2005). In addition, hydroponic systems stimulate the growth and development of pathogens through the highly soluble ions contained in the nutrient solution (Fjallman & Hall, 2005). The water recirculation system used in hydroponics and the climate conditions inside a CEA environment also provide ideal conditions for pathogens to grow and spread (Critten & Bailey, 2002).

While various inspection methods have been developed to identify specific types of plant stresses before visual symptoms appear, the system is still imperfect since it is only able to recognize specific plant stresses. Consequently, human observation is necessary to supplement automated monitoring systems, to ensure that unexpected or unusual disease outbreaks can be recognized early enough to limit damage. A visual inspection system that uses a robotic camera system would permit visual access to inaccessible plants and allows an observer to remotely inspect plants for multiple small or remote CEA operations, whereas a dedicated CEA specialist would be beneficial but impractical under present conditions (Giacomelli, Patterson, & Sadler, 2007).

1.2 Research Objective

The objective of this thesis was to develop a plant inspection robot for use in controlled environment agriculture. The inspection robot should be capable of providing a remote observer with multiple vantage points of each plant to visually assess for signs of plant stress. A preliminary analysis was conducted on the design of this system. The tasks of the research were:

1. Determine the design variables for the plant inspection robot.

2. Define the critical design constraints for this system.
3. Identify a systems-level design process for this system.
4. Determine the design parameters of the system based on the specified design constraints.

1.3 Thesis Outline

The literature review in Chapter 2 describes previously reported plant inspection systems and surveys various farming robots. Chapter 3 describes various structure types and individual components for a Cartesian robotic system. Chapters 4 and 5 present the design variables, design process, and the system specification necessary to satisfy the design constraints for the vision system and motion system, respectively. Chapter 6 concludes and presents the future work in this area.

CHAPTER 2

LITERATURE REVIEW

Whether relying on a human observer or obtaining images necessary for an automated inspection system, it is necessary to develop an imaging system that can move around in a controlled environment and obtain images at the correct resolution and lighting level. Most of the work related to this involves automated inspection or agricultural robotics. For example, researchers have developed vision systems that are capable of accurately discriminating weeds from crops. Other systems use a vision system to estimate a plant's dry weight (Van Henten & Bontsema, 1995), detect calcium deficiency (Story, Kacira, Kubota, Akoglu, & An, 2010), water stress (Kacira, Ling, & Short, 2002), and various specific plant diseases (Chaerle, Hagenbeek, De Bruyne, Valcke, & Van Der Straeten, 2004). Some vision systems can detect these problems before normally noticeable visual symptoms appear. Researchers working in the related area of farming robotics have developed autonomous tractors as well as sophisticated fruit harvesters and precision sprayers. The following sections review both vision systems and agricultural robots.

2.1 Agricultural Vision Systems

There are two types of agricultural vision systems: detection systems and inspection systems. Detection systems are often used in precision spraying applications to detect and discriminate weeds from crops and in harvesting applications to discriminate fruits from leaves and branches. Inspection systems are used to measure plant growth and detect plant stress.

2.1.1 Detection Systems

Detection systems use shape, texture, or color parameters to classify various types of plants (Slaughter D. , Giles, Fennimore, & Smith, 2008) and frequently employ

machine intelligence with learning capabilities in order to deal with the dynamic complexity of unstructured environments (von Wichert, 1998). The selection of the image processing techniques and the classifier algorithm are both important in detection systems. The image processing techniques process the raw image to find features, such as shape outlines and color. The classifier algorithm uses these properties to determine the plant species or whether a particular region of the image represents a fruit or a leaf. If either component of the system fails to perform, the machine vision system will not be able to provide acceptable classification results (Burks, Shearer, & Donohue, 2000). Typically both components must be carefully selected and tuned to a particular problem domain.

Shape-based imaging techniques are able to classify plants with almost 90 percent accuracy in laboratory environments (Woebbecke, Meyer, Von Bargen, & Mortensen, 1995) as well as field tests (Lamm, Slaughter, & Giles, 2002) under ideal conditions**.** However, Slaughter et al. (2008) noted shape-based systems are unable to classify plant leaves that are damaged or occluded because the leaves do not have a characteristic, identifiable shape in such conditions.

Texture-based features are less susceptible to occlusion and are useful in discriminating weeds from crops, achieving accuracies of over 95 percent in laboratory environments. However, texture analysis is computationally intensive (Slaughter, Giles, & Downey, 2008).

Color-based methods are more robust to partial occlusion and generally require less computation than shape-based methods (Slaughter D. , Giles, Fennimore, & Smith, 2008). Color-based methods have shown promise in fruit identification but less so with plant classification. For example, color-based methods can be used to identify Fuji apples with 88 percent accuracy (Bulanon, Kataoka, Ota, & Hiroma, 2002) and eggplants with 67 percent accuracy (Hayashi, Ganno, Ishii, & Tanaka, 2002) when combined with shape-based methods. Burks et al. (2000) noted that color could accurately segment the

plant from the background, but was inadequate for plant classification because leaf orientation with respect to the light source significantly affected the classification accuracy. Other studies contradict this general statement, demonstrating 92 percent accuracy in weed detection of a sugar beet field using color alone (Astrand & Baeveldt, 2002).

Thus, plant detection and identification is an active and promising research area. The inspection system described could provide image input into such a system. This could provide a valuable aid to the human operator by automatically directing attention to unexpected growth in the greenhouse. Ultimately, such a system could perform weed surveillance autonomously. However, since the inputs into the greenhouse are generally controlled, weeds are uncommon and a more frequent problem is ensuring that the expected plants are healthy and growing according to plan.

2.1.2 Inspection Systems

Most automated plant inspection research aims to detect plant stress before the visual symptoms become obvious, since early diagnosis improves prognosis (Chaerle & Van De Straeten 2000). Alaya-Silva and Beyl (2005) noted that hydroponic systems require constant observation because quick decisions must be taken when plants show signs of stress since the plants are entirely dependent on correct water chemistry to survive. Nutrition imbalance can rapidly cause irreparable harm if it is not quickly corrected. In addition, hydroponic systems and the climate conditions inside a CEA environment provide the ideal conditions for pathogens to grow and spread (Critten & Bailey, 2002).

One way to measure plant growth is to use the top-projected canopy area (TPCA), which is the leaf area when viewed from the top of the plant. TPCA correlates linearly to the dry weight of lettuce (Van Henten & Bontsema, 1995). Dry weight is a typical measure of plant size because it is insensitive to the plant morphology and the plant's

water content. When plants grow too quickly, because of too much light relative to the movement of the necessary nutrients to the tips of their leaves, the tips of their leaves turn brown. This is called tip burn. The growth rate obtained by TPCA measurements was able indicate tip burn on lettuce leaves one day before visual symptoms appeared (Story, Kacira, Kubota, Akoglu, & An, 2010). The change in TPCA can indicate water stress 5 to 45 hours before visual symptoms appeared for New Guinea Impatiens grown in low-humidity, high water demand conditions (Kacira, Ling, & Short, 2002).

Other promising techniques include chlorophyll florescence imaging and thermography, which were able detect tobacco mosaic virus on tobacco leaves 38 hours and 35 hours before visual symptoms appeared, respectively (Chaerle, Hagenbeek, De Bruyne, Valcke, & Van Der Straeten, 2004).

Although inspection systems are improving, none have reliably replaced the role of the human in directly observing the plants. While human observers lack the precision of the machine systems, the human visual system is more flexible, particularly for unexpected situations, such as detecting an unusual pest infestation or an unexpected disease. It is likely that even as automated inspection systems grow more reliable, the human observer will never be completely replaced. Ultimately, advanced systems are likely to combine the strengths of both. To some extent, the same is true of agricultural robots.

2.2 Agricultural Robots

Agricultural robots range from large multi-purpose mechanical frames to smaller, autonomous vehicles built for specific applications (Bakker, Asselt van, Bontsema, Muller, & Straten van, 2010). A robot's design is generally determined by the environment in which the robot operates. Outdoor environments generally permit the use of large robots, such as autonomous tractors. However, outdoor robots require sophisticated navigation systems to navigate the unstructured environment. Indoor robots

can take advantage of infrastructure within their environment (Belforte, Deboli, Gay, Piccarolo, & Ricauda Aimonino, 2006). The controlled lighting conditions of the indoor environment also increase the reliability of the vision system (McCarthy, Hancock, & Raine, 2010), which enables the development of more sophisticated farming robots.

2.2.1 Outdoor Robotic Systems

Much of the research activity with outdoor farming robots pertain to navigation, path planning and obstacle avoidance (Pilarski, Happold, Pangels, Ollis, Fitzpatrick, & Stentz, 2002). Over the past decade, this research area has transitioned from controlling a single autonomous tractor to the coordination of multiple autonomous tractors. For example, a recent system can harvest 100 fields of peat moss over a season using three autonomous tractors. Each tractor was able to drive to a field, harvest the peat moss, drive to a designated location and unload it autonomously (Johnson, Naffin, Puhalla, Sanchez, & Wellington, 2009). Other outdoor agricultural robots focus on the farming implement rather than the tractor. For example, towed robotic sprayers can direct nozzles to selectively spray weeds detected by the machine vision system. Such systems have been demonstrated for tomato (Lee, Slaughter, & Giles, 1999) and cotton (Lamm, Slaughter, & Giles, 2002). The selective sprayer developed by Lamm et al. (2002) was able to correctly identify and spray 88 percent of the weeds in a cotton field. Although such systems show great promise, they can only be used in season. Indoor robots can perform their work year-round.

2.2.2 Indoor Robotic Systems

Research in indoor robotic systems is quite active. The high capital costs of a modern greenhouse can justify and facilitate consistent investments, such as robotic systems (Sandini, Buemi, Massa, & Zucchini, 1990). Robots of various complexities have been developed for use in the indoor environment. The most complex and extensively tested robot was a strawberry harvester that used a vision system to assess the

maturity of the strawberry and position the robotic arm to harvest the strawberry. However, it had a successful harvest rate of less than 42 percent, and an average harvesting time of 32.3 seconds, which is 2.5 to 3 times greater than the time required for manual harvesting (Hayashi, Shigematsu, & Yamamoto, 2010). Lower-cost robotic systems based on fixed-position systems have been developed for precision fertilization and spraying (Belforte, Deboli, Gay, Piccarolo, & Ricauda Aimonino, 2006), harvesting (Foglia & Reina, 2006), and mechanical weed control (Belforte, Gay, & Ricauda Aimonino, 2007). The published reports of these systems do not specify how well they performed in a practical sense.

These results suggest that robots can be successfully incorporated into greenhouse operations, but the field is still relatively young and insufficiently explored. In addition, reliability and economic problems represent important challenges for system designers. These problems must be thoroughly addressed for agricultural robots to successfully transition from research to commercialization (Kassler, 2001).

2.3 Economic and Reliability Challenges

Robotic systems have not been fully implemented for a number of reasons including: insufficiently robust and costly mechanical technology, limited working capability of the machine, and low work efficiency. (Kassler, 2001) Further, in an outdoor environment, at least, it is difficult to spread the capital costs across many operations, because most robots are developed for a single application and the need is typically available at only one season (Belforte, Deboli, et al., 2006). The high capital costs of a modern greenhouse can justify and facilitate consistent investments (Sandini, Buemi, Massa, & Zucchini, 1990). Also, with artificial lighting the plants can be managed so that the robot can operate continuously, which can offset the cost of the robot over many operations.

The economic viability of the system is largely determined by the function of the robot. Some agricultural robots are designed for a costly process such as harvesting, which can account for as much as 40 percent of the total cost for horticultural production in the United States (Burks, et al., 2005). A greenhouse inspection robot serves an entirely different economic need. Rather than adding value, it protects against catastrophic loss, by allowing a problem to be detected early. If the availability of the inspection robot allows the greenhouse to be designed without walkways, additional savings can also be obtained through more efficient utilization of the controlled environment, which can be a substantial cost that varies by the square foot. Most of the agricultural production costs are calculated per square foot, so increasing the effective area without increasing the size can have an important impact on the economic viability.

System reliability problems can be largely attributed to robots that rely on multiple complex systems functioning in unison. On a robotic harvester, for example, the vision system must accurately identify fruits, the robotic arm must precisely position the end effector, and the end effector must be able to harvest the fruit without damage. If each of these three sub systems has a reliability of 90% for each fruit, then the probability that none of the systems has a problem (e.g., the probability that each fruit is successfully harvested) is just $(0.9)^3$, or 73%. Reliability can therefore be improved by designing robots with applications that do not require multiple complex systems to function in unison.

2.3.1 Types of Robotic Platforms

There are two distinct classes of robotic platforms: guided vehicle and fixed-position systems.

2.3.1.1 Guided Vehicles

Guided vehicles are used in applications encompassing a large area. Many indoor robotic systems that cover a large area, such as sprayers, use a guided vehicle design. A

guided vehicle follows a fixed trail on the ground of the greenhouse or relies on sensors to navigate through the walkways of a greenhouse. Guided vehicles are able to support large loads, and can travel longer distances than robotic arms and linear motion systems since they do not depend on large overhead structures. The disadvantages are that the walkways must be wide enough to support the robotic system, which reduces the available growing space. The necessary structural modifications to greenhouses to support a guided vehicle can be expensive (Gonzalez, Rodriguez, Sanchez-Hermosilla, & Donaire, 2009) and navigational algorithms can be unreliable (Belforte, Deboli, Gay, Piccarolo, & Ricauda Aimonino, 2006).

2.3.1.2 Fixed-Position Systems

Fixed-position robots have a stationary base or frame, which provides the robot's end effector with a fixed reference frame. This precise and reliable reference is useful in allowing the robot to consistently reach positions within its work envelope. Fixed-position robotic systems are widely used in the manufacturing environment because of their reliability. Most importantly, installation often does not require significant structural modifications.

Fixed-position robots are divided into Cartesian and non-Cartesian systems. Cartesian robotic systems have perpendicular linear actuators that naturally operate in a rectangular frame. Cartesian robots can have a work envelope encompassing acres. Cartesian robotic systems generally do not provide a large range of motion, although it can be coupled with a non-Cartesian robot. This type of robotic platform would be the most ideal for the plant inspection robot since plants are commonly placed in a rectangular area and the camera system does not require a large range of motion to sufficiently inspect the plants. Components and subsystems for Cartesian robots are also readily available, reducing the development cost and time (Belforte, Gay, & Ricauda Aimonino, 2007).

Non-Cartesian robots typically arrange a series of linear or rotation joints in series or in parallel mechanisms. This provides a greater range of motion compared to their Cartesian counterparts. The most common type of a non-Cartesian system is a robotic arm, a series of rotational joints with mechanical links between them. Non-Cartesian systems are used in applications where a complex range of motion is required, such as fruit harvesting and is sometimes a component of a larger robotic system, such as a strawberry harvester (Hayashi, Shigematsu, & Yamamoto, 2010). A robotic arm by itself would not efficiently move across a rectangular space. Since the robotic arm's range of motion is non-rectangular, complex computations are required to calculate the individual joint motions required to create a smooth linear trajectory (Belforte, Gay, & Ricauda Aimonino, 2007). In addition, there are typically several ways to achieve specific positions, leading to multiple solutions to the movement dynamics which must be sorted through in the control system. Non-Cartesian systems, such as the multi-purpose robot built by Belforte et al. (2006) also rely extensively on non-standardized components, which increase both development time and cost and decreases reliability.

2.4 Literature Review Conclusions

The research highlighted here suggests that a plant inspection robot designed for visual inspection is technologically feasible and would provide an unexplored capability to controlled environment agriculture. The research indicates that a variety of plant detection and identification systems have been developed, but most of these are subject to limitations that make them an incomplete solution for industrial growers. These limitations may be best overcome by joining their capabilities with the capabilities of a human supervisor. A survey of a variety of agricultural robots indicates that indoor farming robotic systems are an active research area. The survey also suggests that a Cartesian design is the best-suited structure for a plant inspection robot in a controlled environment with the plants arrayed in rows.

CHAPTER 3

STRUCTURAL AND MECHANICAL DESIGN CONSIDERATIONS

Cartesian robots can take a wide variety of forms and can be constructed from a wide variety of components. The choice of structure and components is largely determined by the accuracy required and the size of the desired work area. The following section describes the principle design choices and how they are connected.

3.1 Cartesian Robotic Structures

The main types of linear motion structures are the cantilever, the column, the moving bridge, the fixed bridge, and the gantry. Cantilever and column structures, illustrated in Figure 1 (a) and (b) respectively, would provide the least obstruction to the plants because they only need to be supported on one side, but these designs cannot span long distances without significant deflection since the z-axis is only supported from one side. A cantilever structure moves the frame along one side. This is practical when the component is heavier than the cantilever structure or when actuating the component is impractical. However, supporting a cantilever beam across a wide greenhouse would require a thick beam to support the large static and dynamic loads. The column structure decouples the z-axis from the x-axis and the y-axis, which could improve accuracy since the inaccuracies in the z-axis will be independent from the accuracy of the x and y-axis. However, in a greenhouse, this arrangement will require the plants to be moved underneath the camera and that requires an empty buffer space as large as the movable plant bed, which would waste considerable greenhouse space.

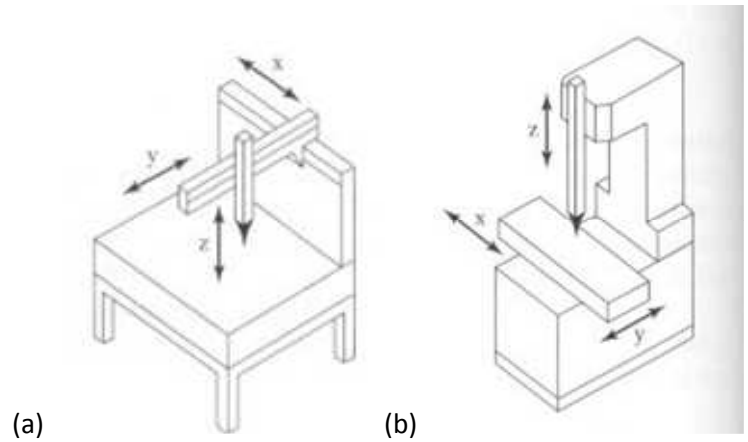

Figure 1: Asymmetrically-supported linear motion structures: cantilever (a) and column (b) (Groover, 2001)

The moving bridge, the fixed bridge, and the gantry-type structures, illustrated in Figure 2 (a), (b), and (c) respectively, are symmetrically supported and can span longer distances without deflection compared to the cantilever and column structures. This structural advantage enables them to have a larger work area. A moving-bridge system actuates the frame while keeping the component stationary. This enables the x-axis to be mounted close to the ground, which is advantageous when the mass of the x-axis mechanism is large compared to the mass of the structure. This structure type is susceptible to yawing, in which the two legs of the bridge move at slightly different speeds, resulting in twisting of the bridge (Groover, 2001). A fixed-bridge structure eliminates this yawing problem by actuating the component instead of the frame. This structure type decouples the x-axis from the y- and z-axis, which can provide greater accuracy since x-axis inaccuracies are independent from the y- and z-axis. Like the column structure, the component is actuated in addition to the frame, which requires a large, empty space in front of and behind the structure to accommodate the table as it moves forward and back. A gantry structure actuates the top section of the bridge rather

than the entire bridge structure, the mobile mass in the x-axis at the cost of the construction of a permanent vertical frame. It also avoids large open paths for the frame rollers that are required for the fixed bridge design. Because of this, a gantry structure is widely used in applications that demand a large indoor working area, where the building's walls and ceilings can subsidize the cost of the structural frame. Consequently, the gantry arrangement is the most effective design arrangement for a plant inspection robot that needs to facilitate the maximum growth area within a fixed structure.

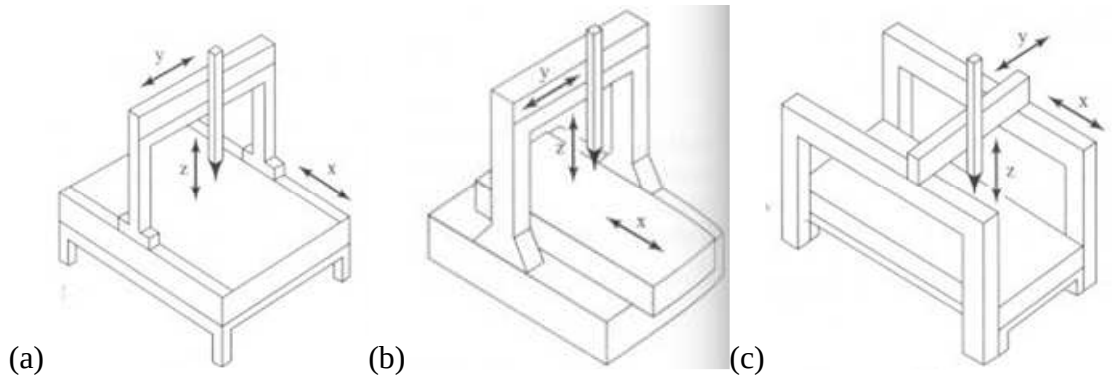

Figure 2: Symmetrically-supported linear motion structures: moving bridge (a), fixed bridge (b) and gantry (c) (Groover, 2001)

3.2 Linear Motion System Components

The gantry arrangement requires a guide system to support both static and dynamic loads, a motor to actuate the system, and a transmission system to convert the rotational motion of the motor into a linear motion. The following sections analyze the design possibilities for each of these arrangements.

3.2.1 Guide System

There are three types of guide systems commonly used in linear motion systems: round rail, profile rail, and v-style rollers. Round rail and profile rail guide systems, shown in Figure 3 and Figure 4, respectively, uses either recirculating ball bearings or a low-friction material to ensure that the linear motion system moves smoothly in the axial direction. Round-rails are generally less expensive, less precise, and support lower loads than profile rails. Profile rails are generally more expensive than round rails and can be more difficult to align. Consequently, profile rails are typically used in applications that have high-load or high precision requirements (Overby, 2010). V-style rollers, shown in Figure 5, use steel wheels with a profiled "V" around the perimeter to support the tangential load. The wheels ride on a hardened steel track with a complementary "V" profile. Although they are not as accurate as the round and profile guides, V-style rollers are easier to implement. Their simple design requires little or no maintenance while providing a long life expectancy. They cost less than round or profile guides, are easier to install and can span long distances (Overby, 2010).

Any guide system provides some friction that the drive motors must overcome in order to move the carriage. Equation (3.1) is used to calculate the frictional force of the guide system, F_{fr} based on the coefficient of friction of the guide system (μ), the mass of the payload (m) and the acceleration due to gravity (g). The maximum payload mass is calculated with Equation (3.2), where F_{R_max} is the maximum load on the guide system, a is the linear acceleration rate, and g is the acceleration due to gravity. This equation assumes that the linear acceleration acts in the same direction as the acceleration due to gravity.

$$F_{fr} = \mu m g \tag{3.1}$$

$$m_{max} = \frac{F_{R\_max}}{a + g} \tag{3.2}$$

Figure 3: Round Rail Linear Bearing System (Glacern Machine Tools, 2012)

Figure 4: Profile Rail Linear Bearing System (Pacific Bearing Company, 2012)

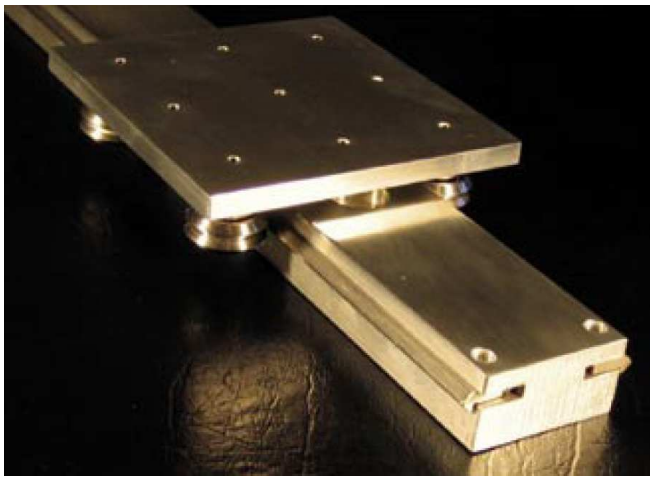

Figure 5: "V"-Style Roller System (Modern Linear, 2004)

3.2.2 Motor

Either stepper or servo motors can be used to provide the power for a linear motion system. Stepper motors are used in precision applications where a high rotational speed is not required. A stepper motor has a large number of magnetic poles in the stator winding that enables the motor to achieve very small increments of rotational movement (Overby, 2010). Common stepper motors are able to provide 200 discrete increments per revolution. Stepper motors are generally driven with an open-loop control structure, meaning the controller assumes that the motor responds as expected to all control signals. This reduces system complexity and the cost of the electronics. To ensure that small force deviations and less-than-ideal operating conditions do not cause the motor to misstep, stepper motors are generally selected to be significantly more powerful than necessary to prevent frequent mismatches between the expected and actual angular position of the stepper motor.

A servo motor drive typically consists of an AC or DC motor integrated with an encoder. The encoder provides position and velocity feedback to the controller. This is

important in applications in which both high linear velocity and high precision are required (Overby, 2010). The controller uses the specific position of the motor provided by the feedback mechanism to determine the best current to send to the motor. The complexity of the controller, the need to tune its control algorithm, and the added cost associated are some of the disadvantages of a servo motor. For both types of motor, torque decreases as angular velocity increases, but a servo motor can reach higher rotational velocities and will generally provide a higher torque at a given rotational speed than a stepper motor, as illustrated in Figure 6.

.

.

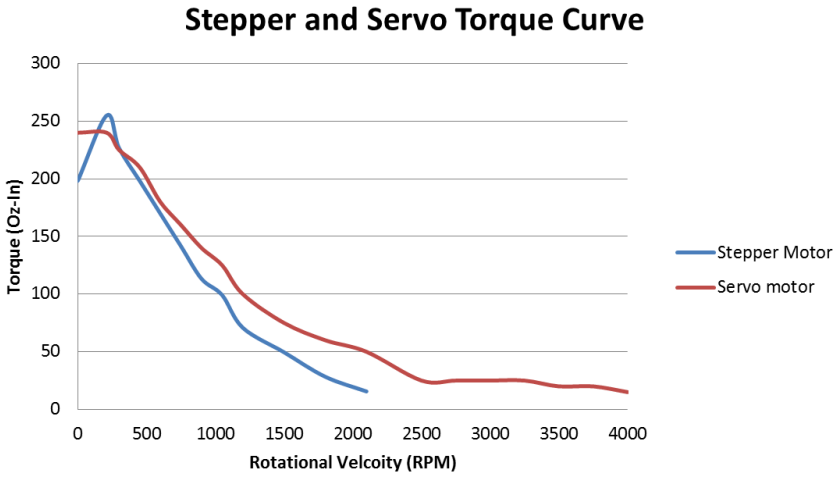

Figure 6: Torque curve of 260 oz-in stepper and 240 oz-in servo

Specifically, torque and rotational velocity requirements from the motor are related to the desired mechanics of the carriage, the system friction, and the design of the transmission.

3.2.3 Transmission

There are two principle types of transmission systems for converting the rotational motion of the motor to the translational motion required for the gantry system: screw-and-nut and rack-and-pinion. These are described below.

3.2.3.1 Screw-and-Nut Mechanism

A screw-and-nut mechanism, shown in Figure 7, is commonly found on small to mid-sized linear motion systems, especially in applications requiring high system resolution. Screw-and-nut mechanisms are limited to small and midsized linear motion systems because the lead screw must be supported at each end. A lead screw spanning a long distance will sag in the middle and can whip along its length. Whip is defined as the amount of deflection away from an axial straight line that the screw will experience, which limits the maximum rotational speed of the system. Because of whip, a longer lead screw will have a lower maximum rotational velocity than a shorter lead screw.

Figure 7: Screw-and-Nut Mechanism (Nook Industries, 2006)

The two principle types of screw-and-nut mechanisms are ball screws and ACME screws. A ball screw uses recirculating ball-bearings to contact the lead screw. It is more expensive than ACME screw-based system but offer higher power transfer efficiencies, accuracy, and longer life expectancy compared to acme screws (Overby, 2010). ACME

screws are not as precise as ball screws and have lower power transfer efficiency, but are significantly less expensive and requires little to no maintenance.

The gearing of a screw-and-nut system is determined by the lead. The lead is the linear distance the nut travels along the screw axis with each revolution of the lead screw. This determines the velocity and force that the nut exerts for a given rotational speed and torque. A large lead provides higher linear velocity, but less force than a smaller lead. Equation (3.3) describes the linear force of a screw-and-nut system given the motor torque (τ), the efficiency of the motion transmission system (η), and the lead (L). The linear velocity is provided by Equation (3.4) with the angular velocity of the motor (ω).

$$F_{motor} = \frac{\tau \times \eta \times 2\pi}{L} \tag{3.3}$$

$$v = \omega \times L \tag{3.4}$$

The resolution of the stepper motor or encoder on a servo motor will limit the resolution of the linear system. The motion system resolution, R_m, for a screw-and-nut system is determined from Equation (3.5), where S is the angular resolution of the motor, given in increments per revolution, and L is the lead.

$$R_m = \frac{L}{S} \tag{3.5}$$

Multiple start lead screws enable a large lead while still facilitating small pitches, which would affect power transfer efficiency. Equation (3.6) is used to determine the lead of lead screws with multiple starts, where n is the number of starts and P is the pitch of the lead screw. The relationship between lead and pitch is shown in Figure 8. Equation (3.7) is used to convert from turns per inch (TPI) to pitch.

$$L = P \times n \tag{3.6}$$

$$P = 1/TPI \tag{3.7}$$

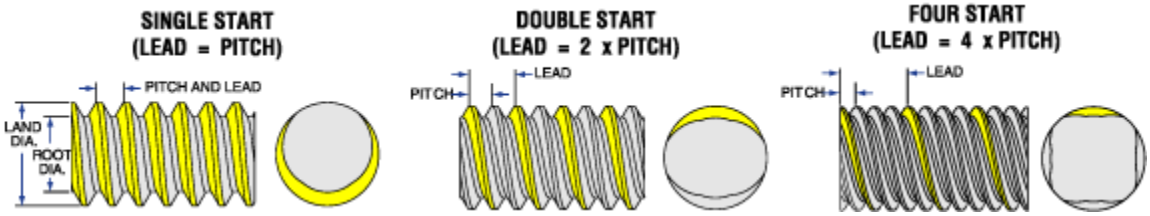

Figure 8: Relation between lead, pitch, and number of starts (Nook Industries, 2006)

3.2.3.2 Rack-and-Pinion System

A rack-and-pinion system, shown in Figure 9, is generally used on linear motion systems that span long distances since the gear rack is continuously supported by the structure, unlike a lead screw, which must be supported only at its ends. Large pinion gears wear more slowly than small ones and offer better power transfer since more teeth are in contact with the gear rack at any given time. However, large pinion gears provide less resolution and decrease the transmitted linear force compared to smaller pinion gears. Gear reduction systems are frequently utilized in rack-and-pinion systems to improve system resolution and to increase the transmitted linear force when large pinion gears are used. Equation (3.8) is used to calculate the linear force applied by a rack and pinion system, F_{motor}, where τ is the torque of the motor, η is the efficiency of the motion transmission system, and P_d is the pitch diameter of the pinion gear. The linear velocity of a rack and pinion system is calculated with Equation (3.9), where ω is the angular velocity of the motor. The system resolution is determined from Equation (3.10), where S is the angular resolution of the motor, given in increments per revolution.

Figure 9: Rack-and-Pinion System (Techno Automation, 2012)

$$F_{motor} = \frac{2 \cdot \tau \cdot \eta}{P_d} \tag{3.8}$$

$$v = \omega \cdot P_D \cdot \pi \tag{3.9}$$

$$R_m = \frac{\pi \times P_D}{S} \tag{3.10}$$

The maximum load of a spur gear is estimated using the Lewis Bending Equation, shown in (3.11), where σ is the bending stress on the gear tooth, W is the face width, Y is the Lewis form factor, $K_v$is the velocity form factor, and P is the diametral pitch of the gear. The Lewis form factor is dependent on the pressure angle and the number of teeth on the gear. The velocity form factor is added to account for dynamic effects of gears. Velocity form factor is calculated with Equation (3.12), where V is the pitch-line velocity in feet per minute (Budynas & Nisbett, 2011). Equation (3.12) assumes that the spur gear has a hobbed or shaped profile. The diametral pitch, a measurement of the number of teeth of a gear per inch of its pitch diameter, is obtained by dividing the number of teeth on a gear (N) by its pitch diameter (P_D), as shown in (3.13).

$$F_{max} = \frac{\sigma WY}{K_v P} \tag{3.11}$$

$$K_v = \frac{50 + \sqrt{V}}{50} \tag{3.12}$$

$$P = \frac{N}{P_D} \tag{3.13}$$

3.2.3.3 Miscellaneous Transmission Systems

While more specialized transmission mechanisms such as chain drives, belt drives, and friction drives can be used for power transmission and offer advantages such as greater acceleration, linear velocity, or accuracy, they can be both expensive and difficult to maintain when scaled to commercial-sized greenhouses compared to a rack and pinion system.

Chain and belt drives are effective in applications where a small payload is moved at high linear velocities with a high acceleration rate over a relatively short distance with a relatively low accuracy (Linear Units Quick Selection Guide, 2012). The mass of the chain or belt increases with distance, making it unsuitable for long traveling distances. Chains and belts also require regular maintenance since chains are susceptible to corrosion and belts are susceptible to stretching.

Friction drive systems, such as a system with powered wheels moving along a flat track, could eliminate the weight associated with a transmission system in low accuracy applications, which is ideal in large work areas. However, this system would require a significant amount of positioning sensors and complex electronics for the system to maintain its accuracy through its range of motion.

3.3 Summary

Because of the configuration of the environment, a plant inspection robot should be based on a gantry design. The gantry could be guided either with a V-groove system,

or a continuously-supported round rail system, depending on the tradeoff between cost and precision required. The drive system could be based on either a stepper motor or servo motor system. The stepper motor design would be less complex, but would require larger motors. The servo system would require feedback from an angle encoder, making it more complex, but would enable a higher system resolution at a given linear velocity. The transmission system could be either a ball and screw system, if the span of the linear rail is short, but a rack and pinion system would be more effective for large spans to avoid whip in the lead screw. The choice of these options would be largely determined by the imaging system and the task of plant inspection.

3.4 Robot Design Overview

An important challenge in designing a complex system, such as the plant inspection robot, is that the design choices made for one subsystem influences the design choices made for the related systems. This leads to complex networks of design interactions that can only be resolved by iterative design methods. Such design approaches can be long and cumbersome compared to designs in which a subsystem can be designed independently to achieve a few optimal performance criteria. Consequently, it is advantageous to divide a large, complex system into relatively independent subsystems, when possible, in order to simplify the design of the subsystems.

The problem of designing a plant assembly robot may be divided into two largely independent sub-problems: the problem of designing an imaging system to acquire images of each plant and the problem of designing a motion mechanism to position the imaging system within the work envelope. Strictly speaking, the problems are interrelated, since the positioning resolution of the motion system puts constraints on the design of the imaging system and the mass of the camera system puts constraints on the motion mechanism. However, as is shown below, the resolution of the motion system has a relatively trivial impact on the design of the imaging system. Consequently, if the

imaging system is designed first, then the mass of the resulting system may be used to design the motion system. The motion system itself can be divided into four largely independent problems of designing the pointing system and each of the three axes, as shown in Figure 10. The motion mechanism contains a pointing mechanism, which is responsible for the pan and tilt of the camera, and the x, y, and z-axis, which are responsible for moving the camera at a particular point in the Cartesian coordinate system. Breaking the large design problem into smaller design problems in this way allows the larger problem to be solved through a largely serial process. The imaging system design will be discussed in detail in Chapter 4and the motion mechanism will be discussed in Chapter 5.

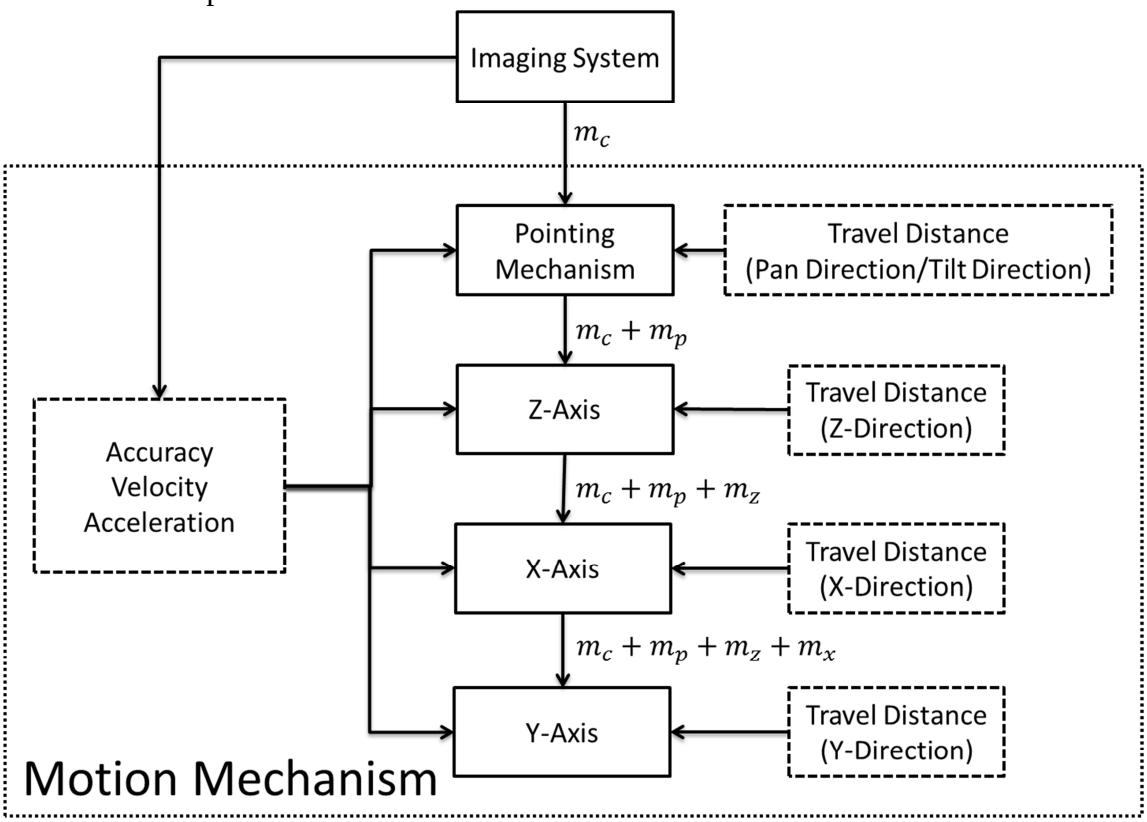

Figure 10: Systems Diagram of the Plant Inspection Robot

3.4.1 Robot Design Assumptions

In order to move towards a specific design, it is necessary to make a number of assumptions that limit the range and scope of the investigation and to anchor certain criteria so that a reasonable range of parameters may be explored. To this end, the imaging system analysis assumes that metal-halide grow lights are used and that the lighting itself has no adverse effects on image quality. In addition, the analysis assumes that there is no mechanical interference between the grow lights and the plant inspection robot.

Also, the motion mechanism analysis focuses on a Cartesian-type gantry design since such a system matches the general geometry of most greenhouses. A round greenhouse, for example, would probably be better served with a different design. Aluminum extrusions were selected as the structural material of this system because of their light density, corrosion resistance, and mounting flexibility. The analysis also assumes that the pointing mechanism and the z-axis motion system will be selected from among available commercial systems, since off-the-shelf solutions are readily available and would likely be a more practical approach than designing a customized solution from scratch. The analysis of the x and y-axis motion mechanism will focus on selection of individual components with an emphasis on scalability.

CHAPTER 4

IMAGING SYSTEM DESIGN

The design challenge for the imaging system is to produce images with sufficient clarity and detail to allow a remote operator to visually inspect the plants. This chapter defines and describes the design variables that influence image clarity and image detail. This chapter also defines a systematic design process for the imaging system with emphasis on the design constraints relevant to a robotic inspection system. From this analysis, specifications for an imaging system appropriate for a plant inspection robot are derived.

4.1 Design Variables

Image clarity is determined by both motion and focus; image detail is determined by the sensor resolution. The effect of motion and focus on image clarity is related to the sensor sensitivity, shutter speed, and aperture size. The effect of focus on image clarity is also related to the sensor size, field of view, and focal length.

4.1.1 Image Clarity

The amount of light necessary to produce a satisfactory image depends on the illumination intensity, sensor sensitivity, shutter speed, and aperture size. The combination of these four parameters yields the exposure value, which determines the amount of light that is captured by the camera. When the illumination intensity is held constant, various combinations of sensor sensitivity, shutter speed, and aperture size will generate the same exposure value, but each parameter will affect the image differently.

The sensor sensitivity determines how well the imaging sensor responds to light. A high sensor sensitivity setting will cause the image to appear brighter, but introduces more noise into the image (Gerlach & Gerlach, 2010). The shutter speed determines the duration of the light exposed on the imaging sensor. A fast shutter speed minimizes

motion blur, but also provides less light to the imaging sensor. The aperture size governs the amount of light that enters the camera at any moment. Smaller aperture opening allow less light into the camera, but improve the focus and depth of field because it reduces distortion caused by off-axis regions of the lens. Aperture size is denoted by an f-number, a dimensionless parameter that defines the ratio between the diameter of the entrance pupil and the focal length; an f-number of 16 means that the entrance pupil diameter is 16 times smaller than the focal length of the lens.

Equation (4.1) defines the shutter speed (t) necessary to capture a good image as a function of aperture size (N), sensor sensitivity (S), object illumination (E_{ob}) and object reflectivity (ρ). C is the calibration coefficient of the light meter.

$$t = \frac{CN^2}{E_{ob} \cdot \rho \cdot S} \tag{4.1}$$

These equations consider only the features in the image plane. It is also important to consider how clearly the object in front or behind the image plane must lie and how far from the focal point the camera must be positioned in order to acquire a clear image. This depends on the both the sensor size and the camera lens.

The sensor size is the physical size of the imaging sensor. A smaller imaging sensor and a lens with a longer focal length may be used to increase the depth of field (DOF), but would require the camera to be placed farther from the object. A small sensor size will increase the DOF but will produce more image noise and reduce the dynamic range compared to a larger imaging sensor with the same resolution, which has a lower pixel density (Allen & Triantaphillidou, 2011). Dimensions of various sensor formats are shown in Table 1.

Table 1: Sensor dimensions and formats employed in digital cameras (Allen & Triantaphillidou, 2011)

Sensor Format	Horizontal (mm)	Vertical (mm)	Diagonal (mm)	Aspect Ratio	Camera Type
1/5	2.6	1.9	3.2	4:3	Mobile Phone
1/2.7	5.4	4.0	6.7	4:3	Compact
1/2	6:4	4.8	8.0	4:3	Compact
1/1.8	7.2	5.3	8.9	4:3	Compact
2/3	8.8	6.6	11.0	4:3	Compact
1	12.8	9.6	16.0	4:3	Compact
1.8	22.2	14.8	26.7	3:2	SLR
1.8	23.7	15.7	28.4	3:2	SLR
35 mm	36.0	24.0	43.3	3:2	SLR/Film

The focal length determines the broadness or narrowness of the imaging angle, which relates the distance between the camera focal point and the field of view, which is the horizontal and vertical area captured by the camera at a given focal distance. A long focal length makes the imaging angle narrow or more telescopic, which effectively increases the focal distance necessary in order to achieve a specified field of view and the depth of field.

Equation (4.2) provides the depth of field as a function of the hyper focal distance (H) and the subject distance (s). The hyper focal distance is the point of focus at which everything from half that distance to infinity falls within the depth of field (Shaw, 1994). Subject distance is the distance from camera at which optimum focus is achieved.

$$DOF \approx \frac{2Hs^2}{H^2 - s^2} \tag{4.2}$$

Both the hyper focal distance and the subject distance depend on the sensor size and focal length. The circle of confusion is the diameter of the circle that results from the object moving towards or away from the camera relative to the plane of sharpest focus.

As the object moves away from the plane of sharpest focus, light from each point on the target object projects to a circular region in the image plane. As the target moves farther from the plane of sharpest focus, this circle grows larger until the target object appears to be “soft” or out of focus. Equation (4.3) defines the hyper focal distance (H) as a function of focal length (f), aperture size (N), and the circle of confusion (c). A reasonable limit for an allowable size for the circle of confusion may be estimated by dividing the diagonal size of the imaging sensor by 1442 (Freeman, 2008).

$$H \approx \frac{f^2}{Nc} \tag{4.3}$$

The maximum subject distance is obtained by equating Equation (4.4) to Equation (4.5) since any distance past D_F, the distance from camera that the image becomes out of focus, would no longer provide sufficient detail even if the image is in focus at that distance. The distance away from the camera necessary to achieve the specified field of view (a) is shown in Equation (4.5), where FOV is the field of view, CCD is the sensor size, and f is the focal length of the lens. Equation (4.5) implies that the field of view changes with distance when the sensor size and focal length is held constant.

$$D_F \approx \frac{Hs}{H - s} \tag{4.4}$$

$$a = f \cdot \left(1 + \frac{FOV}{CCD}\right) \tag{4.5}$$

Equation (4.6) defines the depth of field in terms of basic parameters, where N is the aperture size, f is the focal length, CCD_{Diag} is the diagonal measurement of the sensor size, and FOV_{Diag} is the diagonal measurement of the field of view.

$$DOF = \frac{2Nf\left(CCD_{Diag} + FOV_{Diag}\right)^2}{CCD_{Diag}\left(1442f + 2N\left(CCD_{Diag} + FOV_{Diag}\right)\right)} \tag{4.6}$$

Equation (4.1) and Equation (4.6) show the relationship between the parameters that the inspection images are sufficiently clear. Image resolution must also be analyzed to ensure that the images taken of the plants provide enough information for the remote operator to visually inspect the plants.

4.1.2 Image Detail

The sensor resolution necessary to resolve a small feature is determined by the image field of view and the image's spatial resolution. The number of pixels in an image is the primary determinant of the spatial resolution of an image sensor. A pixel is the smallest unit of information in a picture, and appears as a solid color on a magnified image. Given the same field of view, finer details are captured with a higher resolution imaging sensor than with a lower resolution sensor. However, high-resolution images require more processing time and storage space.

The spatial resolution determines the maximum level of detail available in an image. The size of the smallest object that must be detected or the resolution of a measurement determines the necessary resolution for a particular imaging application. In the case of measurement, the spatial resolution may be better than the projected dimension of a single image pixel. For example, part measurement applications typically use a backlight to illuminate the object, which provides high contrast between the object and the background. A machine vision algorithm can then use changes in brightness to find multiple points along the edge and interpolate the edge's position with a precision equal to 1/3 the size of the area imaged by a single pixel. Detecting abnormalities in an image, such as the presence of a bug on a leaf or an unexpected change in color, require blob and pattern matching algorithms. A blob detection algorithm requires that the abnormality be resolved by several adjacent pixels in order to detect an artifact within a field of random noise. A pattern matching algorithm compares the image taken to a known standard so it requires less information to make the determination. The effective

resolution of many blob detection algorithms is 3 times the imaging area of a single pixel. The effective resolution of a pattern-matching algorithm is approximately the imaging area of a single pixel (Hornberg, 2006).

The spatial resolution (R_s) is determined with Equation (4.7), where S_f is size of the smallest detectable object and N_f is the measurement accuracy of the system. The camera resolution, determined with Equation (4.8) is a function of the spatial resolution of the system (R_s) and camera's field of view (FOV).

$$R_s = \frac{S_f}{N_f} \tag{4.7}$$

$$R_c = \frac{FOV}{R_s} \tag{4.8}$$

4.2 Design Process

Many imaging parameters are interrelated, making it difficult to design an imaging system serially. A tradeoff among parameters for image exposure leads to a conflict in the depth of field, for example. Figure 11 presents a path through the design space that allows a designer to select one parameter and move on to the next to arrive at a satisfactory design. The design constraints of the system are shown in dashed boxes. The dotted box shows the parameters that govern image clarity. Figure 11 show that the field of view governs both image detail and sensor resolution. Image clarity is additionally governed by depth of field, object reflectivity, and illumination. The sensor resolution is additionally governed by inspection detail. Image clarity and sensor resolution parameters are independent of each other.

The design process for the image clarity begins with the selection of sensor sensitivity and shutter speed since their tradeoffs are unable to be compensated by other parameters. Sensor sensitivity should not be changed from the default setting unless absolutely necessary since it would introduce noise into the image, which may mask

image details that are critical to visual plant inspection. Shutter speed is constrained as well because the minimum shutter speed necessary to freeze motion is known. The aperture is therefore the only parameter that could be adjusted to ensure that the image is sufficiently exposed. The appropriate sensor size and focal length must then be chosen to compensate for the aperture size to ensure that the image is still within focus. The specified sensor size, focal length, and field of view will determine the camera distance. The field of view must be increased if the camera distance is unachievable, which will result in a subsequent iteration of this design process.

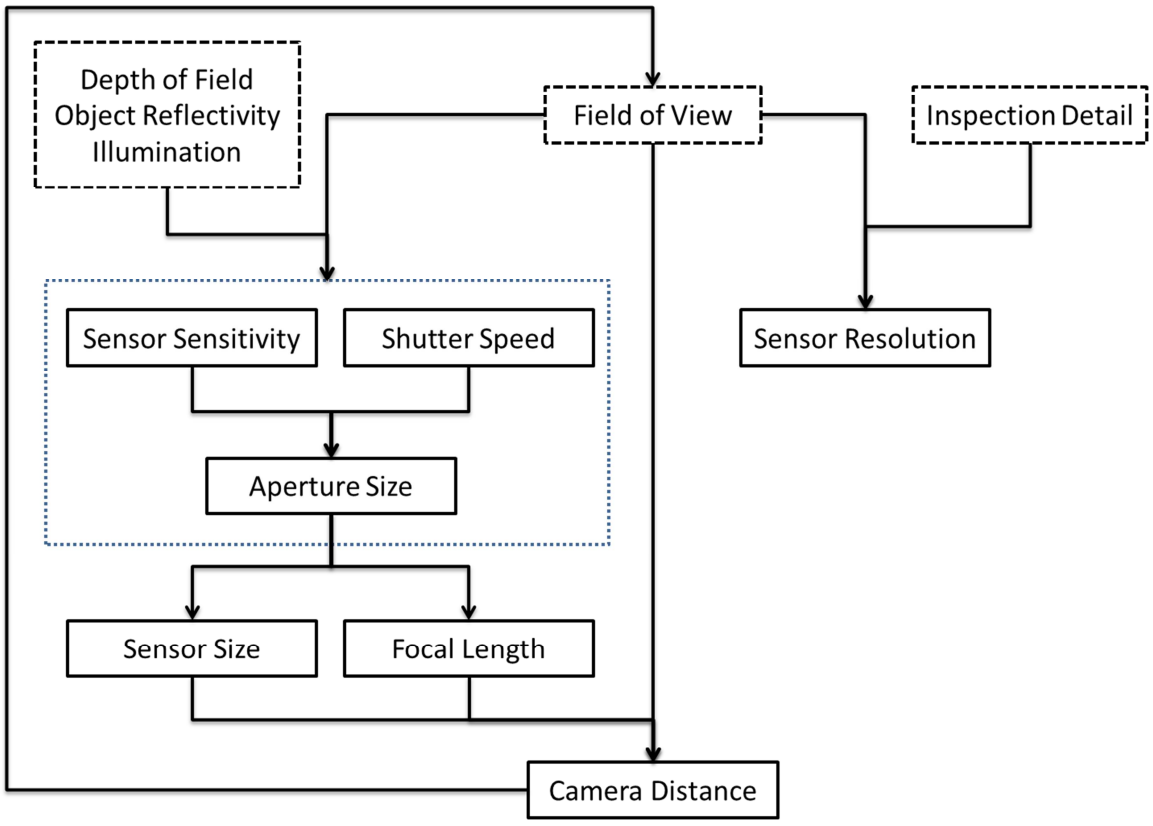

Figure 11: Vision System Design Process

4.3 Defining the Imaging System Design Constraints

This section will explain how the design constraints, listed in Table 2, were defined for the robotic plan inspection imaging system. Generally, each of the constraints relate to the size and shape of the plants to be inspected and the quality of the images necessary to allow for remote inspection.

Table 2: Vision System Design Constraints

Object:	12 inch diameter sphere
Illumination Flux	51420 lux
Shutter Speed (Min)	1/250 second
Sensor Sensitivity (ISO)	100
Minimum Depth of Field	6 in
Diagonal Field of View (Min)	20 inch
Spatial Resolution (Min)	0.01 inch/pixel

4.3.1 Object Shape and Size

For the sake of defining a specific object to be imaged, a head of romaine lettuce was selected. Lettuce inspection was selected as a constraint for this system since it is one of the most popular leafy vegetables in the world. It is frequently cultivated indoors because of its short cultivation cycle from seed to harvest and low light intensity requirement (Okayama, Okamura, Park, et al. 2008). A system capable of romaine lettuce inspection would also be capable of inspecting various smaller lettuce cultivars as well. The average size of a romaine lettuce, the largest common lettuce cultivar, is approximately 12 in diameter. The shape is then abstracted to fall within a sphere with a diameter of 12 in.

4.3.2 Image Exposure

The exposure parameters are governed by the light level, the reflectance of the object, the shutter speed required to avoid motion blur, and the sensor sensitivity. A reasonable value for illumination flux is taken to be 51,420 lux. This value is based on the luminance of a metal halide bulb, a common artificial illumination source in controlled environment agriculture. Specifically the luminance of a 400W bulb was measured at a distance corresponding to its suggested coverage area of 9 ft^2 (Schmidt, 2011).

Air from circulating fans may cause the leaves to move while they are being photographed. Sufficiently freezing motion without a blur requires a shutter speed of $1/250^{th}$ of a second or faster (Finch, 2011). A sensor sensitivity value of 100, the native speed of most digital cameras is assumed since higher sensitivities would introduce more noise into the image (Gerlach & Gerlach, 2010). A sensor calibration constant of 340 and a reflectance ratio of 0.35 for lettuce were assumed for the image exposure calculations (Phan, Brach, & Jasmin, 1979).

4.3.3 Image Focus

The parameters that determine image focus are constrained by the object shape and size, which was selected to be a 12-inch-diameter sphere. The minimal depth of field is 6 in, the radius of the plant. This assumption is based on the idea that the back half of the plant will be obstructed from view and only the front half of the plant needs to be imaged clearly, as illustrated in Figure 12. The minimum vertical field of view must be at least 12 in, the height of the plant. Thus, the diagonal length of the field of view would be 20 in, assuming a standard width to height ratio of 4:3.

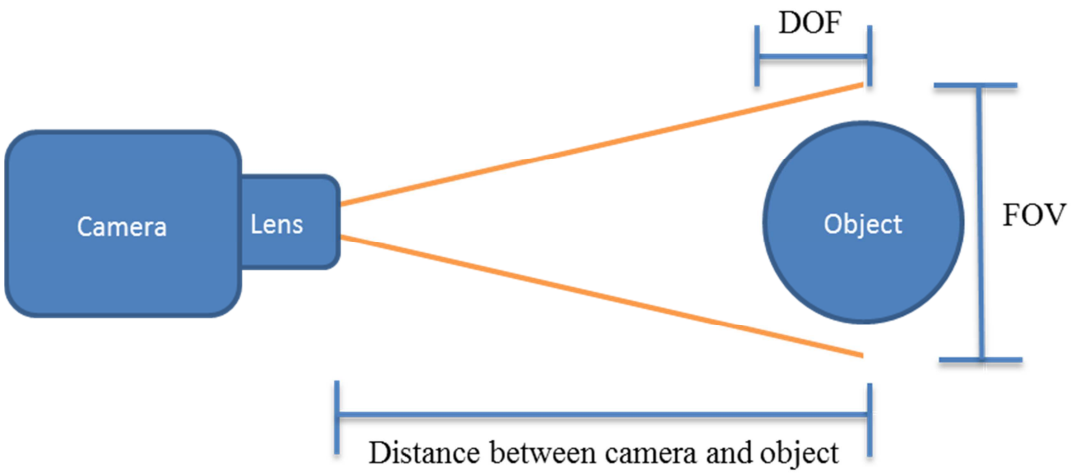

Figure 12: General parameters of a vision system

4.3.4 Image Detail

The image detail requirement is constrained by the size of the smallest feature of interest and the application of the system. The smallest feature of interest in this specific case would be a white fly, a common pest. The average size of an adult white fly is 0.03 in. A blob detection algorithm would be most appropriate for this case, which means that the size of the smallest object must be scaled over 3 pixels, resulting in a spatial resolution of 0.01 inch/pixel when calculated with Equation (4.7) (Hornberg, 2006).

Thus, the above sections describe how each of the design constraints in Table 2 is related to the requirements of the application. These constraints can then be used to define the specific values for each of the parameters, using the procedure defined in Figure 11.

4.4 Design Specifications

The chosen aperture size, focal length, sensor size, and sensor resolution must satisfy the specified design constraints for the vision system to provide sufficient clarity and detail to visually inspect romaine lettuce plants.

4.4.1 Aperture Size

The image exposure calculation shown in Equation (4.1) was used to determine the minimum aperture size necessary to ensure that the image is sufficiently exposed. A minimum aperture opening of f/4 is necessary to satisfy the design constraints described above, as described in Equation (4.9).

$$1/250 = \frac{340N^2}{51420 \cdot 0.35 \cdot 100} \tag{4.9}$$

4.4.2 Focal Length and Sensor Size

The depth of field equation and the constraints of the application described above limit the possible focal lengths and sensor sizes. Equation (4.10) below is derived from the depth of field Equation (4.6), after substituting in the constraints from Table 2. The table indicates that, given the range of sensor sizes listed in Table 3, a sensor format larger than 1/1.8” will not achieve the necessary 6-inch depth of field with a diagonal field of view of 20 in no matter how long the focal length is. Consequently, the largest sensor format that may be used for this application is 1/1.8”. This type of sensor would require a focal length of at least 30.89 mm to achieve the six-inch depth of field. A longer focal length would increase the depth of field.

$$6\ in \cdot 25.4\ mm/in = \frac{2 \cdot 4 \cdot f\left(CCD_{Diag} + (20 \cdot 25.4)\right)^2}{CCD_{Diag}\left(1442f + 2 \cdot 4 \cdot \left(CCD_{Diag} + (20 \cdot 25.4)\right)\right)} \tag{4.10}$$

Table 3: Focal Length for Various Sensor Formats at a Diagonal FOV of 20 in

Sensor Format	Minimum Focal Length (mm)
1/5	1.44
1/2.7	6.5
1/2	13.37
1/1.8	30.89
2/3	Infinity
1.8	Infinity
35 mm	Infinity

4.4.3 Sensor Resolution

Achieving the target resolution of 0.01 in/pixel over the desired field of view requires a minimum resolution of 1600 x 1200 pixels. Equations (4.11) and (4.12), derived from Equation (4.8), demonstrate this calculation, with a 12 in vertical field of view and a horizontal to vertical ratio of four to three. The design specification for this imaging system is shown in Table 4.

.

$$R_{c_{vertical}} = \frac{12\ in}{0.01\ in/pixel} = 1200\ vertical\ pixels \qquad (4.11)$$

$$R_{c_{horizontal}} = \frac{16\ in}{0.01\ in/pixel} = 1600\ pixels\ horizontal \qquad (4.12)$$

Table 4: Imaging System Preliminary Design Specifications

Sensor Sensitivity (ISO)	100
Shutter Speed (s)	1/250
Aperture Size	4
Sensor Type	1/1.8
Minimum Focal Length (mm)	30.89
Minimum Sensor Resolution (pixels)	1600 x 1200

4.5 Design Refinement

A camera system using a 1/1.8” sensor with a resolution of at least 1600 x 1200 would satisfy the design constraints. However, this choice assumes that each plant will be no larger than the nominal 12 in and that the robotic system can place the camera with precise accuracy, so that the camera and view direction will not cause any error. Also, there is the practical problem that the camera must also be placed over 70 in away from the plant to achieve a diagonal field of view of 20 in. Such a long distance would force the movement mechanism to be much larger than it would be if the imaging distance were smaller. The field of view must therefore be increased to reduce the accuracy requirements of the robotic system and to reduce the camera distance.

The necessary increase in the field of view can be determined by various ways such as specifying the desired camera distance or increasing the sensor resolution, which exist in finite increments, while holding the spatial resolution constant. The sensor resolution will be increased incrementally in this case since the robotic system is designed around the imaging system; therefore the camera distance is largely unconstrained.

Increasing the sensor resolution to 2080 x1540, the next available sensor resolution, would allow the viewing angle to be increased. This would provide more flexibility in the absolute precision of the positioning and viewing angle and would allow the system to image plants slightly larger than nominal target. As Equations (4.13) and (4.14) demonstrate, the field of view for this higher resolution sensor is 20.8 in in the horizontal direction and 15.4 in in the horizontal direction. The depth of field would need to be recalculated to determine the focal length of the lens that would be required to achieve newly determined field of view.

$$FOV_{Horizontal} = 2080 \times 0.01 = 20.8\ inch \tag{4.13}$$

$$FOV_{Vertical} = 1540 \times 0.01 = 15.4\ inch \tag{4.14}$$

A minimum focal length of 4.53 mm is required to achieve a diagonal field of view of 25.88 in, as shown in Equation (4.15), which was obtained from Equation (4.6) with the shutter speed, aperture size, and sensor type listed in Table 4. A focal length of 6 mm is the shortest focal length commonly available for use with a 1/1.8 sensor. Equation (4.16) shows that a 6 mm focal length lens will increase the depth of field to 6.74 in. Equation (4.17) shows that a diagonal field of view of 25.88 in is achieved 17.68 in away using a lens with a 6 mm focal length and a sensor format of 1/1.8.

$$6\ in \cdot 25.4\ mm/in = \frac{2 \cdot 4 \cdot f \cdot (8.9 + (25.88 \cdot 25.4))^2}{8.9\left(1442f + 2 \cdot 4 \cdot (8.9 + (25.88 \cdot 25.4))\right)} \tag{4.15}$$

$$\frac{2 \cdot 4 \cdot 6 \cdot (8.9 + (25.88 \cdot 25.4))^2}{8.9\left(1442(6) + 2 \cdot 4 \cdot (8.9 + (25.88 \cdot 25.4))\right)} = 171.23\text{ mm} = 6.74\text{ in} \tag{4.16}$$

$$a = 6 \cdot \left(1 + \frac{657.36}{8.9}\right) = 449.17mm = 17.68\ in \tag{4.17}$$

The camera must be 17.31 +/- 0.37 in from the center of the plant for the camera to remain in focus. The camera should be placed 17.68 in from the center of the plant to permit the largest allowable positioning error. However, the camera should be placed 0.37 in closer to the center of the plant to enable deviations from either direction from

affecting the image focus. The final design specification for the camera system is shown in Table 5.

Table 5: Imaging System Design Specifications

Sensor Sensitivity (ISO)	100
Shutter Speed (s)	1/250
Aperture Size	4
Sensor Type	1/1.8
Minimum Focal Length (mm)	6
Sensor Resolution (pixels)	2080 x 1540
Field of view (in)	20.8 x 15.4
Depth of Field (in)	6.74 in

4.6 Camera Selection

There are three major classes of cameras available: consumer-grade digital cameras, web cameras, and industrial cameras. Most consumer digital cameras have a sensor resolution that is higher than specified and are relatively inexpensive. However, these cameras are not natively able to provide pictures in real-time into the computer for processing. Substantial programming time may be needed to seamlessly integrate a consumer digital camera into machine vision software. The integration of the camera and lens makes these systems inflexible when adapting them to new applications. In addition, moving parts such as the zoom lens assembly would make the camera less reliable for calibrated measurements. Web cameras can provide real-time images in real-time into the computer for processing and often come with capabilities that allow the camera to be controlled in real time. However, no webcams were found with a resolution that is higher than 1600 x 1200 pixels. Machine vision cameras are typically designed for integration

with machine vision software. Also, they are usually designed with a lens mount, which enables the lens to be selected separately from the imager. A fixed focal length will also be more durable since it limits the number of moving parts.

Most industrial cameras are in the 2 megapixels and 5 megapixels range. The AVT F-320, shown in Figure 13, was one of the few machine vision cameras that have a 3 megapixel resolution, which translates to 2080x1540 pixels. The AVT F-320 industrial camera uses a standard c-mount lens. The Edmund Optics NT67-709 6 mm fixed-focal length lens, shown in Figure 14 is one of many standard c-mount lenses that would suffice the design specifications. This system has a weight of 1 pound (AVT Oscar Firewire.A Cameras, 2012) (Compact Fixed Focal Length Lenses, 2012). Although this system will theoretically suffice for visual lettuce inspection, it is important to understand the limitations of such a system.

Figure 13: AVT F-320 Machine Vision Camera

Figure 14: Edmund Optics NT67-709 6mm fixed-focal length lens

4.7 Design Limitations

Illumination presents the most critical limitation of the vision system. A brighter conventional light source would enable faster shutter speeds to prevent motion blur and a larger depth of field to increase image focus. However, brighter lights would also increase energy consumption and could present adverse effects on the plant, such as tip burns due to excess heat. Grow lights based on light-emitting diodes (LED), which use a fraction of the power compared to traditional light sources, may adversely affect visual plant inspection since the plant leaves would appear gray under LED-based grow lights because it contains only blue and red LEDs.

Data processing speed is another potential limitation of the vision system. Cameras with a higher sensor resolution will produce images with greater detail than cameras with lower resolution. However, the high-resolution images require longer processing times and consume more storage spaces. In addition, the connection between the camera and the computer contains a finite bandwidth, which limits the speed at which images may be transferred from the camera to the computer. Higher-resolution images would therefore be transferred to the computer at a slower rate.

In summary, the challenge of designing an imaging system for plant inspection can be solved with an off-the-shelf camera and lens combination. The proposed solution meets or exceeds all of the design requirements and would provide clear images of any plant that can fit inside a 12” spherical volume. The next chapter describes the factors that need to be considered when designing a system to position and point the camera.

CHAPTER 5

MOTION MECHANISM DESIGN

The design challenge for the motion mechanism is to carry and reliably position the imaging system while achieving the necessary velocity, acceleration, and accuracy throughout the work envelope. The velocity and acceleration will affect the inspection time. The accuracy will affect the image quality, in that the pointing precision will depend on the mechanism's ability to repeatedly and precisely place the camera in a specific position. The motion mechanism consists of two sub-mechanisms: the positioning system and the pointing mechanism. The positioning system includes the large, structural frame that will move the camera payload to a given position within the Cartesian work envelope. The pointing mechanism will ride on the positioning system and will point the camera at a given plant.

This analysis focuses primarily on the positioning system, which is the more complex design problem, since the pointing system can be purchased as a complete unit. This chapter defines and describes the design variables that influence velocity, acceleration, and accuracy. The chapter also examines the impact that velocity, acceleration, and accuracy have on the motion mechanism design and the relationships among the design parameters. From this analysis, specifications for a motion mechanism appropriate for the plant inspection robot are derived.

5.1 Design Considerations

The following sections provide definitions for the mechanism velocity, acceleration, and position accuracy.

5.1.1 Design Parameters

The motion mechanism's linear velocity determines the maximum number of plants that can be inspected within a specified time period. The motion mechanism's

acceleration rate determines the travel distance necessary to reach the desired velocity. Equation (5.1) shows the relationship between the velocity and the number of plants that can be inspected, where n_p is the number of plants, t_p is the required time for the robot to complete its inspection, d is the diameter of the plant, and l is the distance between the camera and the center of the plant. The distance traveled is determined by the plant spacing and the circumference of the path around the plant with a radius that is the distance from the camera to the center of the plant. The minimum plant spacing in a hydroponic environment would be the diameter of the plant (d), which would assume that the plants are just touching one another when the plants are fully grown.

A graphical representation of Equation (5.1) is shown in Figure 15 where the solid line represents the diameter of the lettuce plant, the dashed line represents the circular trajectory of the camera and the dotted line represents the linear trajectory used to inspect subsequent plants. One of several possible camera trajectories described by Equation (5.1) for inspecting multiple plants is shown in Figure 16.

.

$$v = \frac{n_p(2\pi l + d)}{t_p} \tag{5.1}$$

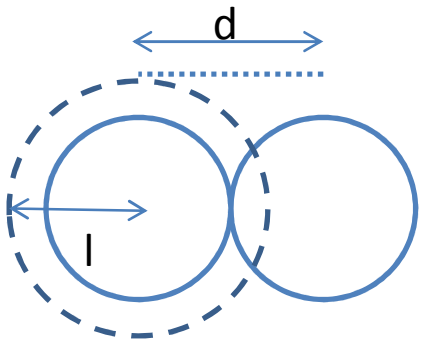

`

Figure 15: Diagram of camera trajectory described by Equation (5.1)

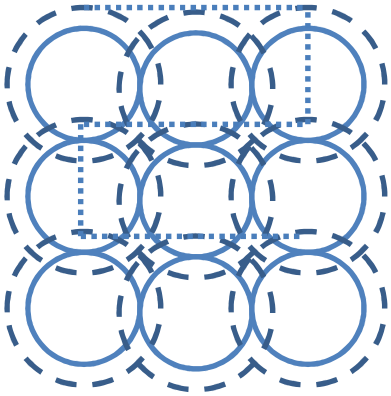

Figure 16: Diagram of camera trajectory for multiple plants

One of the possible methods used to determine acceleration rate is shown in Equation (5.2), where a is the acceleration rate, v is the desired linear velocity and l_a is the distance necessary to reach the desired velocity. Equation (5.2) assumes that the linear velocity increases linearly throughout distance l_a and the mechanism is accelerating from a standstill. In addition to velocity and acceleration, system accuracy also affects the mechanism design.

$$a = \frac{v^2}{2l_a} \tag{5.2}$$

5.1.2 System Accuracy

The system accuracy depends on the accuracy of two subsystems: the pointing mechanism and the positioning system. The positioning accuracy ensures that the image remains in sufficient focus. The pointing mechanism accuracy ensures that the plant is centered in the image and is therefore appropriately cropped.

5.1.2.1 Camera Pointing Mechanism Accuracy

The pointing mechanism accuracy required to properly image a target depends on the object size, the field of view, and camera distance. The accuracy requirement can be relaxed with a shorter camera distance. Allowing for lots of border in the image, such as imaging a small object in a large field of view will also relax the accuracy requirement for the pointing mechanism. For a spherical object, the accuracy in the vertical direction is more sensitive than the horizontal direction since the vertical field of view is generally smaller than the horizontal field for view for most digital imaging formats in their standard (landscape) orientation.

The allowable error for the tilt axis of the camera ($\varepsilon_{\theta V}$) can be estimated from the difference between the angle of view based on the vertical field of view (β_V) and the angle of view based on the object diameter (α), as shown in Equation (5.3), where FOV_V is the field of view in the vertical direction, d is the diameter of the lettuce plant, and l is the distance between the camera and the object. This relationship is illustrated in as shown in Figure 17. The allowable error for the pan axis of the camera ($\varepsilon_{\theta H}$) is determined identically as the tilt axis, as shown in Equation (5.4), where FOV_H is the field of view in the horizontal direction.

$$\varepsilon_{\theta V} = \beta_V - \alpha = 2(\tan^{-1}\left(\frac{0.5\ FOV_V}{l}\right) - \tan^{-1}\left(\frac{0.5d}{l}\right)) \quad (5.3)$$

$$\varepsilon_{\theta H} = \beta_H - \alpha = 2(\tan^{-1}\left(\frac{0.5\ FOV_H}{l}\right) - \tan^{-1}\left(\frac{0.5d}{l}\right)) \quad (5.4)$$

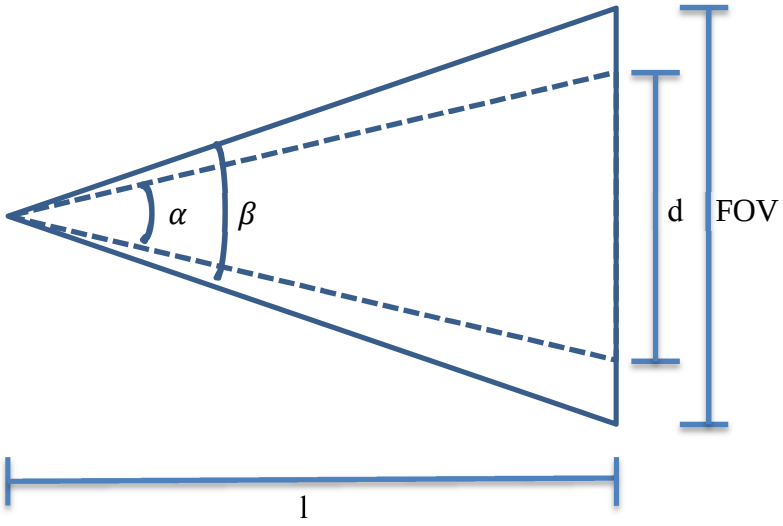

Figure 17: Vertical Angle of View of the Object Height and Vertical Field of View

5.1.2.2 Positioning Mechanism Accuracy

The positioning mechanism accuracy is affected by the structural deflection as well as the accuracy and resolution of the guide and transmission system. The root sum-square (RSS) method, shown in Equation (5.5), defines the system's positional accuracy, where ε_x, ε_y, and ε_z are the errors associated with the x, y, and z-direction, respectively. The RSS method assumes that the system errors are independently distributed and follow a Gaussian distribution (Figliola & Beasley, 2006).

$$\varepsilon = \sqrt{\varepsilon_x^2 + \varepsilon_y^2 + \varepsilon_z^2} \tag{5.5}$$

For simplicity, the error components in each direction are also assumed to be independently distributed and are also combined with the RSS method. Equation (5.6) defines the error components as combination of the structural deflection (D_i), linear motion system resolution (R_{m_i}), and the transmission and guide system accuracy (ε_{t_i})

in direction i. Equation (5.7), substitution of Equation (5.6) into Equation (5.5), shows the errors that would determine system accuracy for a 3-axis Cartesian robot.

$$\varepsilon_i = \sqrt{D_i^2 + R_{m\_i}^2 + \varepsilon_{t\_i}^2} \tag{5.6}$$

$$\varepsilon = \sqrt{D_x^2 + R_{m\_x}^2 + \varepsilon_{t\_x}^2 + D_y^2 + \varepsilon_{r\_y}^2 + R_{m\_y}^2 + D_z^2 + R_{m\_z}^2 + \varepsilon_{t\_z}^2} \tag{5.7}$$

5.1.2.3 Structure Deflection

For the reasons provided in Section 3.1, a gantry design is selected as the best general structure for the plant inspection system. This section defines the critical design parameters for the general gantry system arrangement illustrated in Figure 18.

.

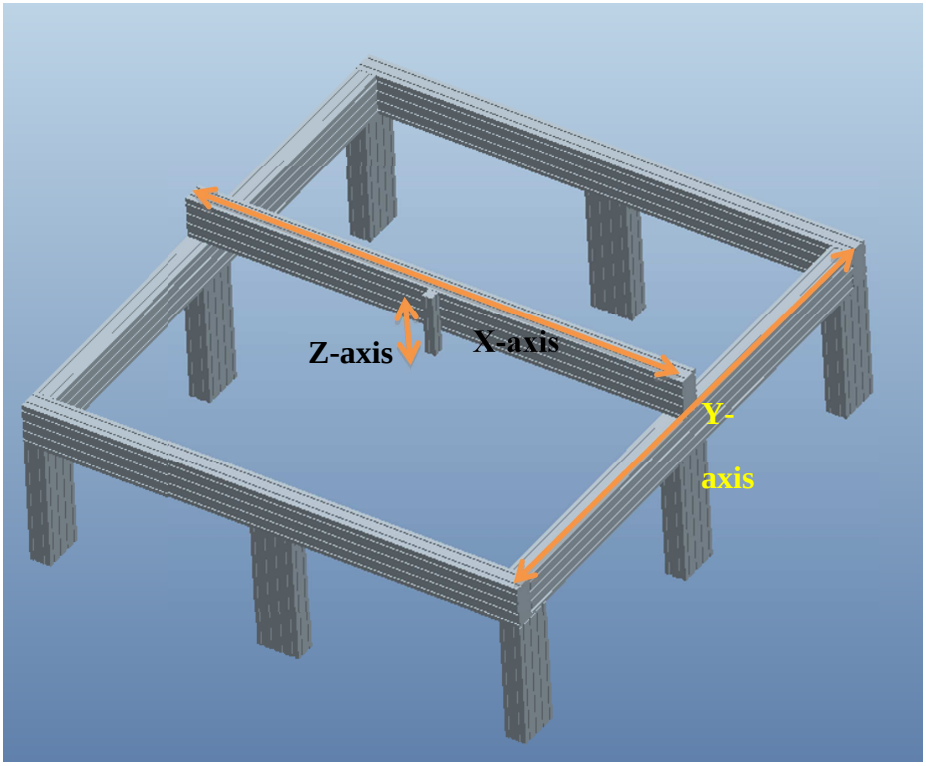

Figure 18: Gantry-style analyzed for the plant inspection system

The key design criterion for the structure is its ability to support the elements of the camera and the motion mechanism without deflecting. Although the structure can theoretically deflect in many different directions, the principle design problem is to avoid the deflection of the large x-axis span, which must support the weight of the camera at its middle. The y-axis bears more weight than the x-axis, but it may be easily reinforced to reduce the magnitude of the deflections, whereas the x-axis beam cannot be reinforced. Consequently, this analysis focuses on the total deflection of the camera position in the z-direction.

In the worst case, this deflection is the sum of the deflections in the direction of each of the component axes. For example, Equation (5.8) expresses the error in position of the payload in the z direction as a function of the z-direction deflection of the z axis, plus the z-direction deflection of the y axis and the z-direction deflection of the x axis. Since the deflection in the z-axis is an axial load on the structural member, D_{z_z} is negligible. The deflection of the y-axis in the z-direction (D_{z_z}) is considered negligible as well since the y-axis can be reinforced. Consequently, $D_z \approx, D_{z\_x}$.

$$D_z = D_{z\_x} + D_{z\_y} + D_{z\_z} \tag{5.8}$$

The worse-case deflection of x-axis is illustrated in Figure 19. The deflection would be less if the translational joints were designed to resist torsion than if the joint was simply supported at its ends. If, however, the axis is represented as a simply supported beam with a point load in the middle, Equation (5.9) provides the standard formula for the deflection of the beam as a function of its length, L, the weight of the load, W, the modulus of elasticity of the material, E, and the second moment of inertia, I, which is determined from the shape and cross-sectional dimensions of the structure member.

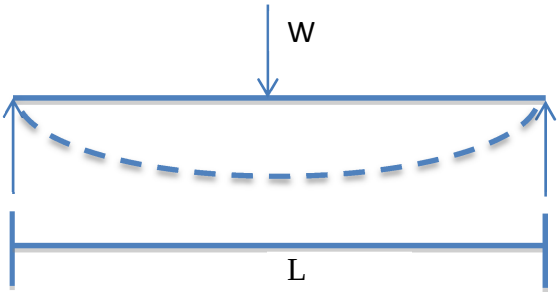

Figure 19: Diagram of a simply supported beam with length (L) with load (W)

$$D = \frac{L^3 \cdot W}{48 \cdot E \cdot I} \tag{5.9}$$

For simplicity, the weight of the z-axis components, the movement mechanism mounted on the x-axis, and the weight of the x-axis beam itself are all included in the point load. This is a conservative estimate, since the weight of the beam is a distributed load and the motion components will be displaced from the center. However, these simplifying assumptions allow Equation (5.10) to express the deflection of the x-axis in the z direction as a function of the weight of the components on the x-axis (w_x) and the weight of the z-axis (w_z), and the weight of the beam itself. The weight of the beam is determined from material density (ρ), the distance between the supports in the x-axis (L_x), and cross sectional area (A) of the material. The weight of components on the x-axis includes the weight of the motor, the guide system, and transmission system that actuates the z-axis in the x-direction.

$$D_{z\_x} = \frac{(w_x + w_z + \rho_x L_x A_x) L_x^3}{48EI} \tag{5.10}$$

The deflection of the y-axis in the z-direction occurs at both ends of x-axis structure. Each side may be represented as a simply supported beam in a situation analogous to Figure 19 above. Each of the two structural members of the y-axis must

support half the weight of the x-axis, the weight of the components on the y-axis and the weight of the y-axis structural member itself, as shown in Equation (5.11). The weight of components on the y-axis includes the weight of the motor, the guide system, and transmission system that actuates the x-axis in the y-direction. This calculation assumes that the structure members of the y-axis are simply supported, although these members could be reinforced.

$$D_{z\_y} = \frac{(w_y + \rho_y L_y A_y + 0.5(w_x + w_z + \rho_x L_x A_x))L_y^3}{48EI} \tag{5.11}$$

5.1.3 Motor Torque

The torque applied by the motor is directed through the transmission system to accelerate the motion of the camera payload in space. Some of the torque is lost to friction within the guide system and the transmission, and also to accelerating components within the transmission itself.

Equations used to determine the motor torque are specified in terms of pitch diameter for ease of calculation. The lead could be converted into an equivalent pitch diameter if a screw-and-nut mechanism is used since both of these parameters are used to specify the linear distance traveled per rotation.

Equation (5.12) shows that the linear force provided by the transmission must overcome the frictional force (F_{fr}) of the guide system and the acceleration force (F_a) necessary to actuate the load to the desired velocity. The total force necessary to move the payload for a linear motion system is shown in Equation (5.13), where μ is the coefficient of friction of the guide system, m is the mass being actuated, g is the acceleration of gravity, and a is the acceleration rate of the system. The necessary torque to actuate the system is calculated in Equation (5.14), where P_d is the pitch diameter of the transmission system and η is the efficiency of the transmission system. Equation

(5.14), obtained by substituting Equation (5.13) into Equation (3.8), assumes that the torque necessary to overcome the rotational inertia of the drive system is negligible.

Besides an understanding of the design parameters and equations that govern the motion mechanism design, it is important to understand the relationships among the design parameters since it governs the structure and motion design.

$$F_{tot} = F_{fr} + F_a \tag{5.12}$$

$$F_{tot} = \mu mg + ma \tag{5.13}$$

$$\tau_{total} = \frac{P_d}{2\eta}(\mu mg + ma) \tag{5.14}$$

5.2 Design Overview

Designing the mechanical motion mechanism is a complex task because many of the design decisions are influenced by other design decisions, as illustrated in Figure 20. For example, the mass of the pointing mechanism must be accounted for when designing the z-axis. Therefore, the interdependencies of the different elements of the design must be considered in the design of the final system to minimize iterative design solutions.

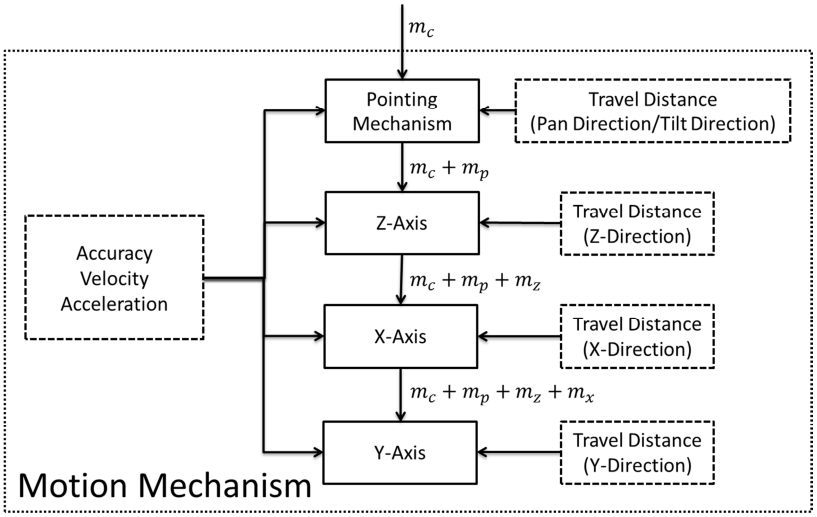

Figure 20: Motion Mechanism Systems Diagram

5.2.1 Design Process

The systems diagram for the motion mechanism illustrated in Figure 20 shows that the pointing mechanism is specified first, followed by the z-axis, x-axis, and y-axis since the mass of the precedent sub-system must be accounted when designing the subsequent sub-system. The dashed boxes in Figure 20 indicate the design constraints for the motion mechanism. All the sub-systems are influenced by the accuracy, velocity, and acceleration specification. The travel distance must also be specified for each sub-system. The design constraints, however, must be specified first to adequately design each sub-system.

5.2.2 Design Constraints

The motion mechanism design must satisfy the design constraints for its functionality to not be compromised. Specifically, the system accuracy would affect image focus and image cropping while the work area, velocity, and acceleration would affect the inspection time. The design constraints for the motion mechanism, explained in detail in subsequent sections are listed in Table 6.

Table 6: Motion Mechanism
Design Constraints

	Accuracy
Focus	17.31 +/- 0.37 in
Cropping	+/- 8.8 inch (h)
	+/- 3.4 inch (v)
	Travel Distance
X-Axis	244 in
Y-Axis	244 in
Z-Axis	17.31 in
Pan	360 degrees
Tilt	90 degrees
	Velocity and Acceleration
Velocity	97 in/min
Acceleration	130.68 in/s^2

5.2.2.1 Accuracy

The imaging system design specifies that the camera must be 17.31 +/- 0.37 inch from the center of the plant for the image to be in focus, which results in a maximum system error of 0.74 inch. This imaging system provides a horizontal field of view of 20.8 in and a vertical field of view of 15.4 in, which enables a deviation of 8.8 inch deviation from the center of the image in the horizontal direction and a 3.4 inch deviation from the center of the image in the vertical direction for the 12 inch diameter lettuce plant to remain within the camera's field of view.

5.2.2.2 Travel Distance

The size of the greenhouse and its layout would most likely constrain the size of the plant inspection robot and therefore the length of the x-axis and the length of the y-axis. The number of plants to be inspected combined with the structural layout could also

be used to determine the size of the inspection robot. Costs would increase non-linearly with work area since there is a cubic relationship between structural deflection and its length. A longer structure would therefore weigh significantly more, contributing to added material costs. Higher linear velocity and acceleration rates are also required to ensure that the images of the plants are captured in the specified timeframe, which would require stronger motors.

For the sake of this analysis, since this robot was not designed for a pre-existing greenhouse, the longest standardized length of aluminum extrusion would be used for the x and y-axis, which is 242 in. The z-axis requires a minimum travel distance of 17.31 in from the camera to obtain the side and top view of each plant while ensuring that the images remain in focus. The motion mechanism requires the camera to pan 360 degree to image the plant from all sides and tilt 90 degrees to image both the top and sides of each plant.

5.2.3 Velocity and Acceleration

The linear velocity for the x-axis and y-axis is calculated with Equation (5.1) based on the number of plants to be inspected (n), plant diameter (d), camera distance (l), and inspection time (t). A plant diameter of 12 in was specified in the imaging system design constraints. The imaging system specification determined a camera distance of 17.31 in. Equation (5.15) shows that a 242 inch long structural member has a usable length of 17 ft. once camera distance is accounted for, resulting in a total coverage area of 289 square feet in a gantry-type configuration. Therefore, this plant inspection robot is capable of inspecting 289 romaine lettuce plants assuming that the plants are placed in 1ft x 1ft grids. An arbitrary inspection time of 6 hours is specified to enable the robot to inspect the plants more than once per day, if necessary. Equation (5.16) shows that a linear velocity of 97 in per minute is required to satisfy these parameters.

$$242 - 2 \cdot 17.31 \approx 17\ ft \tag{5.15}$$

$$v = \frac{289(2\pi \cdot 17.31 + 12)}{60 \cdot 6} = 97\ ipm \tag{5.16}$$

The acceleration rate for the x and y axis is largely application-dependent. No literature was found on general guidelines for determining the appropriate acceleration rate on a Cartesian robot. An acceleration distance of 0.01 inch was therefore selected to reach the desired linear velocity. Equation (5.17), obtained by substituting the linear velocity calculated in Equation (5.16) into Equation (5.2) along with an acceleration distance of 0.01 inch shows that an acceleration rate of 11 ft/s^2 is necessary to 97 in/min from a standstill in 0.01 inch. This equation assumes that the linear velocity is increased linearly. The 11 ft/s^2 acceleration rate is consistent with CNC mills with a similar linear velocity.

$$a = \frac{(97/60)^2}{2 \cdot 0.01} = 130.68\ in/s^2 \tag{5.17}$$

The velocity and acceleration for the z-axis is not as critical because actuation in the z-direction is unlikely since the top of each plant is captured through the multiple side view. It is recommended that velocity and acceleration for the z-axis to be similar to the velocity and acceleration of the x and y-axis to enable the camera to travel from the side to the top of the plant concurrently, if necessary.

5.3 Motion Mechanism Design

5.3.1 Pointing Mechanism Design

The pointing mechanism is responsible for pointing the camera at the individual plants. The pointing mechanism must be capable of actuating the imaging system, which has a weight of 1 lbs, while satisfying the design constraints specified above. Cropping of the images may occur if this system does not satisfy the specified design constraints shown in Figure 21.

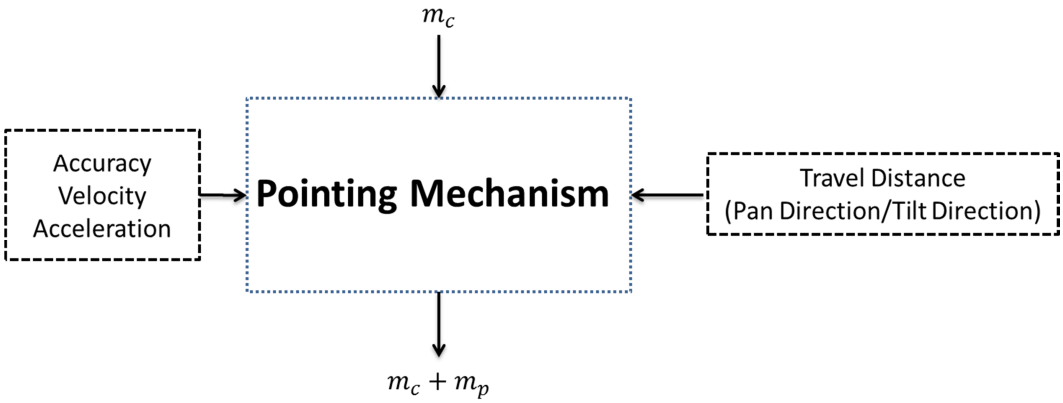

Figure 21: Pointing Mechanism Systems Diagram

5.3.1.1 Velocity and Acceleration

The angular velocity and acceleration for the pointing mechanism must be proportional to the velocity and acceleration of the x, y, and z- axis since the image may be cropped if the linear velocity of the x, y, and z-axis is faster than the rotational velocity of the pointing mechanism.

The rotational velocity and acceleration of the pan axis depends on the linear velocity and acceleration of the x and y-axis while the rotational velocity and acceleration of the tilt axis depends on the linear velocity and acceleration of the z-axis. Equations (5.18) and (5.19) show the pan axis needs to travel at an angular velocity of 321 deg/min with an angular acceleration rate of 432.6 deg/s^2, with the given linear velocity of 97 in/min and linear acceleration of 130.68 in/s^2, when the camera is 17.31 in from the center of the plant. This rotational velocity and acceleration applies to the pan axis as well since the same linear velocity and acceleration is specified for the z-axis.

$$\omega = \frac{97\ in/min}{17.31\ in} = 5.6\frac{rad}{min} = 321\ deg/min \quad (5.18)$$

$$\propto = \frac{130.68\frac{in}{s^2}}{17.31\ in} = 7.55\ \frac{rad}{s^2} = 432.6\ deg/s^2 \quad (5.19)$$

5.3.1.2 Accuracy

Equations (5.20) and (5.21), obtained by substituting the vertical field of view of 15.4 in and camera distance of 17.31 in into Equation (5.3) and a horizontal field of view of 20.8 in and a camera distance of 17.31 in into Equation (5.4) shows that the tilt and pan axis has an allowable error of 28.8 degrees and 42.9 degrees respectively. This error calculation assumes that the camera is perfectly positioned in the Cartesian axes.

$$\varepsilon_{\theta V} = 2(\tan^{-1}\left(\frac{0.5 \cdot 15.4}{17.31}\right) - \tan^{-1}\left(\frac{0.5 \cdot 12}{17.31}\right)) = 28.8\ deg \quad (5.20)$$

$$\varepsilon_{\theta H} = 2(\tan^{-1}\left(\frac{0.5 \cdot 20.8}{17.31}\right) - \tan^{-1}\left(\frac{0.5 \cdot 12}{17.31}\right)) = 42.9\ deg \quad (5.21)$$

5.3.1.3 Design Requirements

Based on the analysis conducted above, the pointing mechanism must support a 1 lbs payload, rotate 360 degrees in the pan-axis and rotate 90 degrees in the tilt axis at an angular velocity of 321 deg/min and an angular acceleration of 432.6 deg/s^2. The pan and tilt axis requires an accuracy requirement of 42.9 degrees and 28.8 degrees, respectively.

5.3.1.4 Desirable Features

The pointing mechanism should be easily controlled by a computer to integrate it with the positioning mechanism. The pointing mechanism should also be as light as possible to minimize structure weight and motor size.

5.3.1.5 Mechanism Selection

While various integrated solutions that contain the pointing mechanism and imaging system exist, the integration of the camera and lens makes these systems inflexible when adapting them to new applications. For this reason, a separate pointing mechanism is used for the camera. Table 7 shows a selection of pan and tilt mechanisms that may be applicable for this application. Pan and tilt systems that are designed for large cameras and systems that cannot be integrated with a computer are not included in the table. Of the systems surveyed, the Eagle PT-50, FLIR PTU-D46, PTU-D100, PTU D48E, and Servo City DDT500 mechanisms would satisfy the design constraints. The Servo City DDT500, Eagle PT50, and FLIR PTU-D46 would be the best options based on weight of the mechanism.

Of these three options, the Servo City DDT500, shown in Figure 22, which is actuated by hobby servos, is the pointing mechanism that is the best-suited for this application since it is the lightest mechanism. Although this system is lower in accuracy compared to the other systems, the accuracy is still within the design constraints. Hobby servo motors are also easily interfaced with the computer.

Table 7: Selection of Pointing Mechanisms

Brand	Model	Max Load (lb)	Pan Motion (deg)	Tilt Motion (deg)	Velocity (deg/s)	Accuracy (deg)	Weight (lb)	Communication
Eagle Pan Tilt Systems	PT-50	6	360	90	18	0.16	8	RS-232
Fujinon	CPT-70F-02A	8.8	300	190	20	0.5	5.1	RS-232
Frezzi	FPT-25	25	354	180	35	0.1	10	RS-232
FLIR	PTU-D46	6	360	111	300	0.05	3	RS-232
FLIR	PTU-D100	20	360	120	120	0.008	21	RS-232
FLIR	PTU-D48E	15	360	120	100	0.006	11	RS-232
Servo City	DDT500	2	36	180	100	1	1	Microcontroller

Figure 22: Servo City DDT-500 Pan/Tilt Mechanism

5.3.2 Z-Axis

A standardized off-the-shelf linear motion system can be used on the z-axis since the design requirements does not place any constraints that cannot be satisfied with a pre-made system. The systems diagram of the z-axis is shown in Figure 23. This diagram assumes that a complete linear motion axis is selected instead of individual components. The type of transmission system (i.e. ball screw or ACME lead screw) may be specified for these systems.

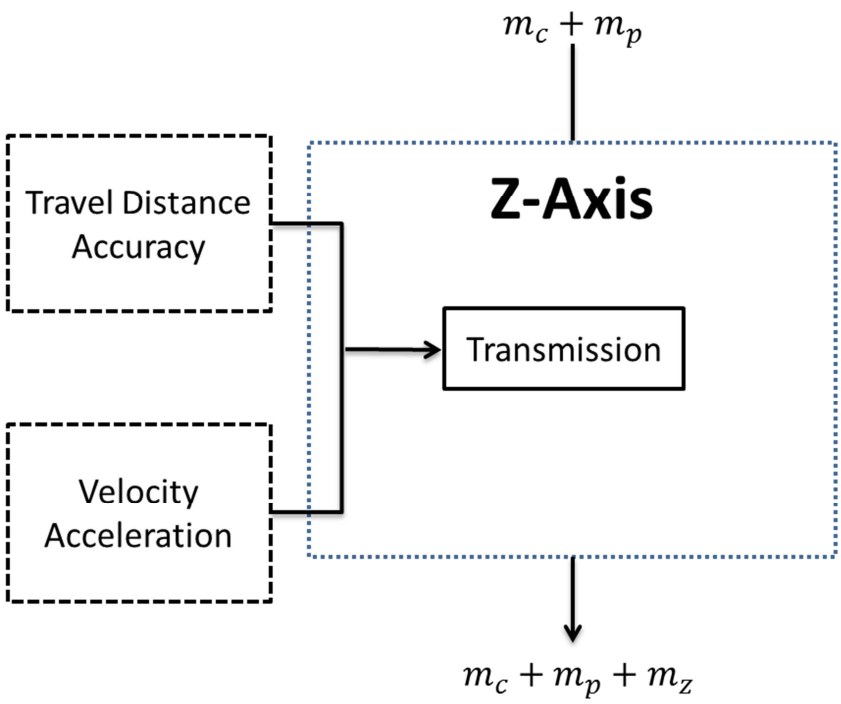

Figure 23: Systems Diagram of Z-axis

5.3.2.1 System Requirements

Based on the design constraints of the motion mechanism, the z-axis requires a minimum travel distance of 17.31 in and must support a payload of 2 lbs, with the imaging system and pointing mechanism each having a weight of one pound. A linear velocity of 97 ipm and an acceleration rate of 130.68 in/s^2 are desired. Equation (5.22) shows that the z-axis is required to handle a dynamic load of 2.7 lbs when the desired acceleration rate is accounted.

$$F_{D\_x} = \frac{2\ lb}{32.2 ft/s^2} * 10.89 \frac{ft}{s^2} + 2\ lbs = 2.68\ lbs \qquad (5.22)$$

5.3.2.2 Desirable Features

The z-axis should be as light as possible to minimize motor size and structure weight.

5.3.2.3 Z-Axis Selection

Anaheim Automation, Parker Automation, and USAutomation all manufacture linear actuators that will suffice for this application based on the travel distance and dynamic load requirement, as shown in Table 8. The accuracy of the z-axis is an order of magnitude smaller than the system accuracy requirement, therefore it is considered negligible. Of these systems, the Parker Automation LP28, shown in Figure 24, is the only system that achieves the desired linear velocity. This system has a weight of 3 lbs.

Table 8: List of Linear Actuators

Brand	Model	Dynamic Load (lb)	Travel Distance (in)	Accuracy (in)	Max Velocity (ipm)	Transmission Type	Weight (lb)
Anaheim Automation	LS100-18	25	18	0.005	60	Ball Screw	9.25
Parker	LP28	11	19.7	0.002	106	Lead Screw	3
USAutomation	UST8020-18	200	18	0.0108	60	Lead Screw	9.5

Figure 24: Parker LP28 Electronic Positioner

Other manufactures such as PBC linear, Thomson Automation, THK, Techno-Isel, and Macron Dynamics, and Nook Industries manufacture linear actuators to custom specifications, which are not needed for the z-axis since a pre-built solution is available, which would save cost.

5.3.3 X-Axis Design

Although pre-built systems are available for the x-axis for the desired length, a component-based solution is analyzed so this approach may be used to design plant inspection robots with different work areas.

The systems diagram for the x-axis, illustrated in Figure 25, shows that the transmission and guide systems are defined by travel distance, accuracy, velocity and acceleration; the structure is defined by the travel distance and accuracy; the motor is defined by the velocity and acceleration. This diagram shows that the transmission and

guide systems can be designed in parallel, but the motor and structure must be designed sequentially after the design of the guide and transmission system since the mass of the motor is accounted when designing the structure.

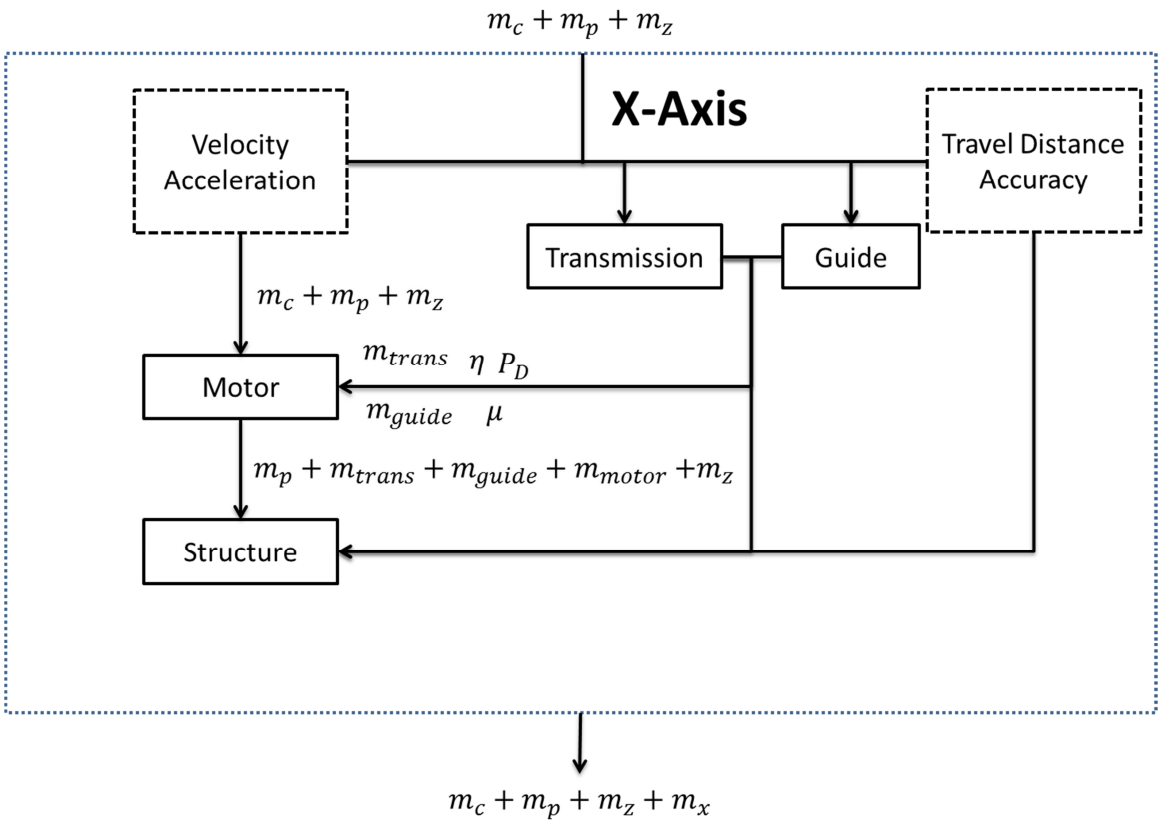

Figure 25: X-axis Systems Diagram

5.3.3.1 Design Requirements

A travel distance of 244 in, accuracy of 0.74 inch, linear velocity of 97 ipm and an acceleration rate of 130.68 in/s^2 are required for this system. The systems has to support a weight of 5 lbs, consisting of a 1 lbs imaging system, 1 lbs pointing

mechanism, and a 3 lbs z-axis positioning mechanism. Equation (5.23) specifies that a dynamic load (F_{D_x}) of 6.7 lbs must be supported by the system.

$$F_{D\_x}\frac{5\ lb}{32.2 ft/s^2} * 10.89\frac{ft}{s^2} + 5\ lb = 6.7\ lbf \tag{5.23}$$

In addition to the dynamic load, the system resolution would need to be defined. The system resolution defines the linear distance traveled per rotational increment of the servo or stepper motor. The system resolution therefore presents a tradeoff between motor torque and linear velocity. A higher system resolution results in a larger force and a lower maximum linear velocity. Lower system resolution would require less structural deflection for the system to remain within specification.

The system resolution for the plant inspection robot is negligible with regards to its effects to structural deflection since the system is allowed a very large error. Equation (5.24) shows that a pitch diameter of 0.125 inch is required for the system to reach the desired 97 ipm when the motor rotates at 250 rpm, which is the approximate rotation speed of the motor at peak torque output for both stepper and servo motor, as shown in Figure 6, and is at the lower end of the motor's rotational velocity. Equation (5.25) shows that a pitch diameter of 0.125 in had a negligible effect on the system accuracy at 200 increments per revolution, the most common resolution for stepper motors. Servo motors are capable of higher angular resolutions.

$$P_D = \frac{97}{250 \cdot \pi} \approx 0.125\ in \tag{5.24}$$

$$\sqrt{\left(\frac{0.125\pi}{200}\right)^2 + \left(\frac{0.125\pi}{200}\right)^2 + D_z^2 + \left(\frac{0.125\pi}{200}\right)^2} \leq 0.74 \tag{5.25}$$

Since the pitch diameter of 0.125 inch is negligible with regards to the allowable deflection, this system could be optimized for a higher linear velocity or a smaller motor to lower operating cost. This design will be optimized on the usage of a smaller motor

since there are no profound advantages of a faster inspection time for this specific application.

A torque curve for the motor is therefore necessary to determine the rotational speed and pitch diameter combination that would yield that largest force output. A motor type must be selected to determine the optimal pitch diameter since stepper and servo motors have different torque curves. A stepper motor is recommended for this application because high rotational velocities are not required since high system resolutions are not required. Using a stepper motor would eliminate cost and complexity associated with a servo drive system. Table 9 shows the pitch diameter necessary to reach a linear velocity of 97 ipm at the specified rpm and the force output based on the torque curve and the specified pitch diameter. Table 9 shows that the peak force at 97 ipm occurs at approximately 700 rpm, which requires a pitch diameter of 0.044 in. This analysis assumes that other stepper motors have an identical torque profile as the Probotix HT23-260-4 stepper motor.

Table 9: Pitch Diameter and Force at Velocity of 97 ipm

Rotational Speed (rpm)	Torque (oz-in)	P_d (in)	Force (oz)
225	240.72	0.137	3508.3
300	226.56	0.103	4402.6
400	207.68	0.077	5381.1
500	188.80	0.062	6114.6
600	169.92	0.051	6604.0
700	151.04	0.044	6848.8
800	132.16	0.039	6848.3
900	113.28	0.034	6604.0
1000	99.12	0.031	6420.5
1100	84.96	0.028	6053.6
1200	70.80	0.026	5503.3
1300	63.72	0.024	5365.7
1400	56.64	0.022	5136.4
1500	49.56	0.021	4815.4

5.3.3.2 Guide System Design

The distance requirement for the x-axis eliminates the use of end-supported linear bearing systems because it will be exposed to excessive deflections. However, continuously-supported round rails guide systems, profile rail guide systems, and v-groove guide systems are not subjected to length constraints since the rails can be mounted end-to-end to extend length. The desired acceleration and linear velocity are all within the limits of these guide system types.

While all three of these guide systems would work for this application, a v-groove bearing system is recommended since this application places a larger emphasis on debris, maintenance and corrosion than accuracy, which is on the order of several thousands of an inch. Roller bearings are assumed to have a coefficient of friction of 0.014 (Kent, 1916). PBC Linear, Bishop Wisecarver, Modern Linear, and VXB Bearings are some of

the major suppliers of v-groove guide systems. Since comparable products are available from multiple manufactures, V-groove bearings made by Bishop Wisecarver will be used for this analysis because of its information availability and selection size. These v-groove bearings are capable of a maximum linear velocity of 196 in/s (Bishop Wisercarver DualVee Catalog, 2010). This analysis process can be applied to other suppliers of guide systems. Relevant specifications for this analysis from Bishop Wisecarver for various models are shown in 10.

Table 10: V-Groove Bearing Specifications (Bishop Wisercarver DualVee Catalog, 2010)

Part No	Wheel Size	Wheel Diameter (in)	Radial Load (lbf)	Axial Load (lbf)	Bearing Weight (lb)	Track Weight (lb/ft)
W1SSX	1	0.771	274	57	0.025	0.183
W2SSX	2	1.21	596	141	0.086	0.343
W3SSX	3	1.803	1326	382	0.287	0.69
W4SSX	4	2.36	2181	900	0.608	1.1
W4SSXXL	4XL	2.968	3215	1473	1.27	1.1

Table 10 shows that a wheel size of 1 is sufficient to support the z-carriage on the x-axis since it has a maximum radial load of 274 lbf, which is significantly more than the required 6.7 lbf. This particular gantry system can carry a maximum mass of 6.34 slugs, at the desired acceleration rate, as calculated with Equation(5.26), obtained by substituting the desired acceleration rate of 11 ft/s^2 and the maximum radial load of 274 lbf into Equation (3.2). The weight of this track is 3.7 lbs, as calculated in (5.32). The weight of the bearings is negligible.

$$m = \frac{274\ lbf}{11\ ft/s^2 + 32.2\ ft/s^2} = 6.34\ slugs \qquad (5.26)$$

$$w_{track} = 0.183 \cdot 242\ in/12\left(\frac{in}{ft}\right) = 3.7\ lb \qquad (5.27)$$

5.3.3.3 Transmission Selection

The distance requirement for the x and y axis eliminates the use of nut-and-screw transmission systems because of whip. A rack-and-pinion system is recommended for use on the x and y-axis since it provides minimal rotational inertia and is designed to transverse long distances since the gear racks can be placed end-to-end. A rack and pinion system typically has an efficiency of 80 % (Funakubo, 1991).

For the purpose of this analysis, commonly available rack and pinion sizes from Boston Gears, one of the leading manufacturers of rack and pinion systems will be analyzed. The rack and pinion selections are based on the standard parts available from Grainger Industrial Supply since standard sizes are unavailable from the manufacturer. This rack and pinion system has a pressure angle of 14.5 degrees. The three smallest sizes of gear racks along with its pitch and weight are shown in Table 11. The lightest gear rack will be analyzed first to minimize weight. The lightest gear rack in Table 11 has a face width of 0.375 in and a pitch of 20. Spur gears with 12 to 32 teeth are available in a pitch of 20 (Boston Gear Power Transmission Parts, 2012). Equation (5.28), derived from Equation (3.12), shows that the velocity form factor at a linear velocity of 97 ipm is 1.197. Equation (5.29) shows that this rack and pinion system can sustain a maximum force of 151 lbf, assuming a tensile strength of 90,000 psi for stainless steel, a safety factor of 3, a face width of 0.375 in, a form factor of 0.322 (32 teeth spur gear with 14.5 degree pressure angle), and a velocity form factor of 1.197. This gear rack weighs 17.54 lbs at a span of 242 in, as calculated in Equation (5.30). The maximum force of this rack and pinion system exceeds the specified requirement.

Table 11: Common Gear Rack Sizes
from Boston Gears

Face Width (in)	Pitch	Weight (lb/ft)
0.3125	16	1.28
0.375	20	0.87
0.75	12	2.0

$$K_v = \frac{50 + \sqrt{97}}{50} = 1.197 \tag{5.28}$$

$$F_{max} = \frac{(90000/3)(0.375)(0.322)}{1.197 \cdot 20} = 151\ lbf \tag{5.29}$$

$$w_{rack} = 0.87\ lb/ft \cdot \frac{242\ in}{12\ in/ft} = 17.54\ lb \tag{5.30}$$

The 32 teeth spur gear has a pitch diameter of 1.6 in. Thus, a gear reduction mechanism is necessary to reduce the pitch diameter to the desired diameter of 0.044 inch. Equation (5.31) shows that a gear ratio of 36:1 is necessary to obtain the desired pitch diameter.

$$Gear\ Ratio = \frac{1.6}{0.044} \approx 36 \tag{5.31}$$

One of the gearboxes that would work is the Thomson Linear NT23-030 Planetary box, which has a 1:40 gear ratio, a weight of 1.9 lbs, a maximum torque output of 207 lb-in, and an efficiency of 88 %. The equivalent pitch diameter would be 0.04 inch, as shown in (5.32). Other planetary gearboxes that have a gear reduction of approximately 36:1 will work for this application as well.

$$P_D = \frac{1.6}{40} = 0.04\ in \tag{5.32}$$

Based on this analysis, the guide system chosen has a weight of 3.7 lbs and a maximum radial load of 274 lbs. The transmission system consists of a rack and pinion system that weighs 17.54 lbs and carries a maximum load of 151 lbs. The gear reducer has a weight of 1.9 lbs. The total weight of the guide and transmission system for the x-axis is thus 23.14 lbs.

5.3.3.4 X-Axis Motor

The motor on the x-axis has to actuate a total weight of 5 lbs, consisting of the weight of the imaging system, pointing mechanism, and the z-axis. The motor should provide a linear velocity of 97 ipm, acceleration rate of 10.89 ft/s^2. Equation (5.33) shows that the motor needs to provide a 1 oz-in of torque to actuate the object, with an 80 % factor of safety, a 0.04 in equivalent pitch diameter, 80 % efficiency for the transmission system, and 88 % efficiency for the gear reduction mechanism.

$$\tau_{total} = \frac{0.04}{2(0.8)(0.8)(0.88)}\big(0.014(5) + 5/32.2\ ft/s^2(11\ ft/s^2)\big)\left(16\frac{oz}{lb}\right) = 1\ oz - in \tag{5.33}$$

Equation (5.34) shows that the motor must have a rotational velocity of at least 772 rpm at the desired torque to provide the desired linear velocity of the x and y-axis.

$$N = \frac{97}{0.04\pi} = 772\ rpm \tag{5.34}$$

Any stepper motor that provides at least 1 oz-in of torque at 772 rpm will work for the x-axis. One of the stepper motors that meets this specifications is the Anaheim Automation 08Y202 stepper motor, shown in Figure 26, which provides approximately 2.4 oz-in of torque at 772 rpm, as shown in Figure 27. This motor has a weight of 0.13 lbs.

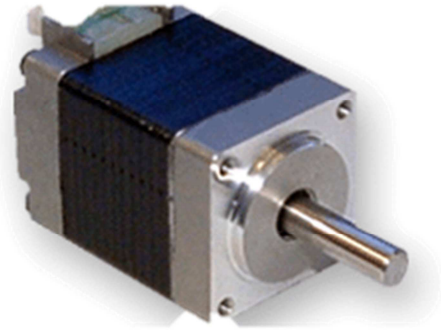

Figure 26: Anaheim Automation 08Y202 Stepper

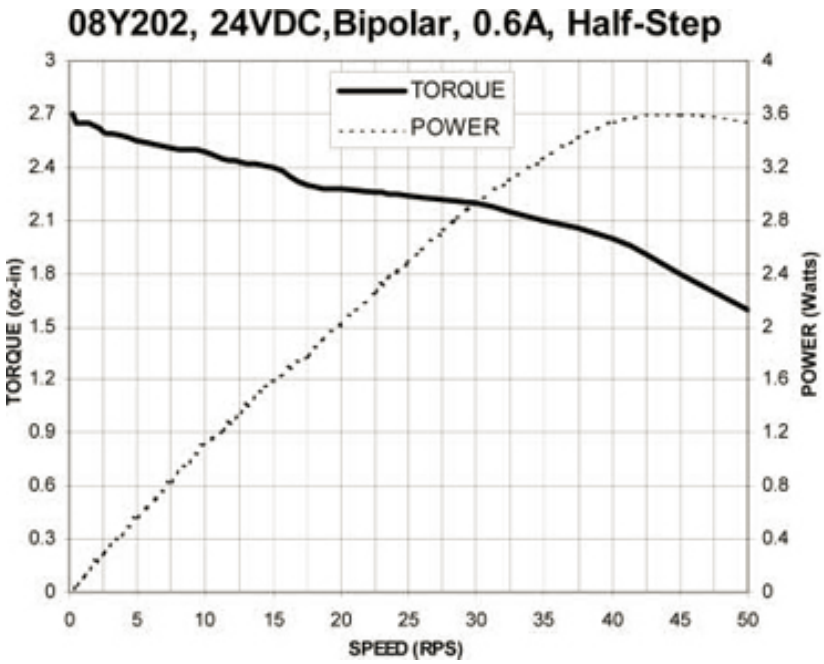

Figure 27: Anaheim Automation 08Y202 Torque Curve

5.3.3.5 Structure

The structure must support 28.27 lbs, consisting of the 5 lbs payload weight carried by the x-axis along with the weight of the guide and transmission system, which has a combined weight of 23.14 lbs, and the weight of the motor, which is 0.13 lbs. A maximum deflection of 0.74 in is allowed in the z-direction. The deflection of the z-axis is considered negligible since the axis is axially loaded. Thus, the deflection of the x-axis and y-axis in the z-direction should be less than 0.74 in. The deflection of the x-axis is of higher priority than the deflection of the y-axis since the y-axis can be reinforced.

For the purpose of this analysis, aluminum structural extrusions available from 80/20 Inc. are analyzed. Table 12 shows all extrusions except model 1010 would deflect less than 0.74 in under the given load. Model 1020 is recommended for use since it is the lightest structure, at a weight of 18.6 lbs. The deflection of the model 1020 extrusion at 28.27 lbf is 0.44 in. Deflections were calculated with Equation (5.10) with the values given in Table 12.

Table 12: Deflection Calculations of Aluminum Extrusion for X-axis

Model	Ix (in^4)	Iy (in^4)	A (in^2)	Weight (Lb/Ft)	Length (in)	weight (lb)	E (PSI)	Force (lb)	D (in)
1010	0.0442	0.0442	0.4379	0.5097	242	10.28	1E+08	28.27	2.525
1020	0.08333	0.3078	0.7914	0.9212	242	18.58	1E+08	28.27	0.441
1030	0.1238	0.9711	1.1596	1.3498	242	27.22	1E+08	28.27	0.165
2020	0.5509	0.5509	1.2079	1.406	242	28.35	1E+08	28.27	0.298
2040	1.0513	3.5168	2.2462	2.6146	242	52.73	1E+08	28.27	0.067
1515	0.2542	0.2542	1.154	1.3433	242	27.09	1E+08	28.27	0.630
1530	0.4824	1.8042	2.0798	2.4209	242	48.82	1E+08	28.27	0.124
3030	3.4133	3.4133	3.4477	4.0131	242	80.93	1E+08	28.27	0.093
3060	6.5164	22.03	6.4262	7.4801	242	150.85	1E+08	28.27	0.024

5.3.4 Y-Axis

The design of the y-axis is similar to the design of the x-axis in terms of the components used and design requirements. Consequently, the systems diagram of the y-axis, shown in Figure 28, is identical to the systems diagram of the x-axis, except that the mass of the x-axis must now be considered. However, two of this system is used, one to support each end of the x-axis to prevent asymmetric loadings.

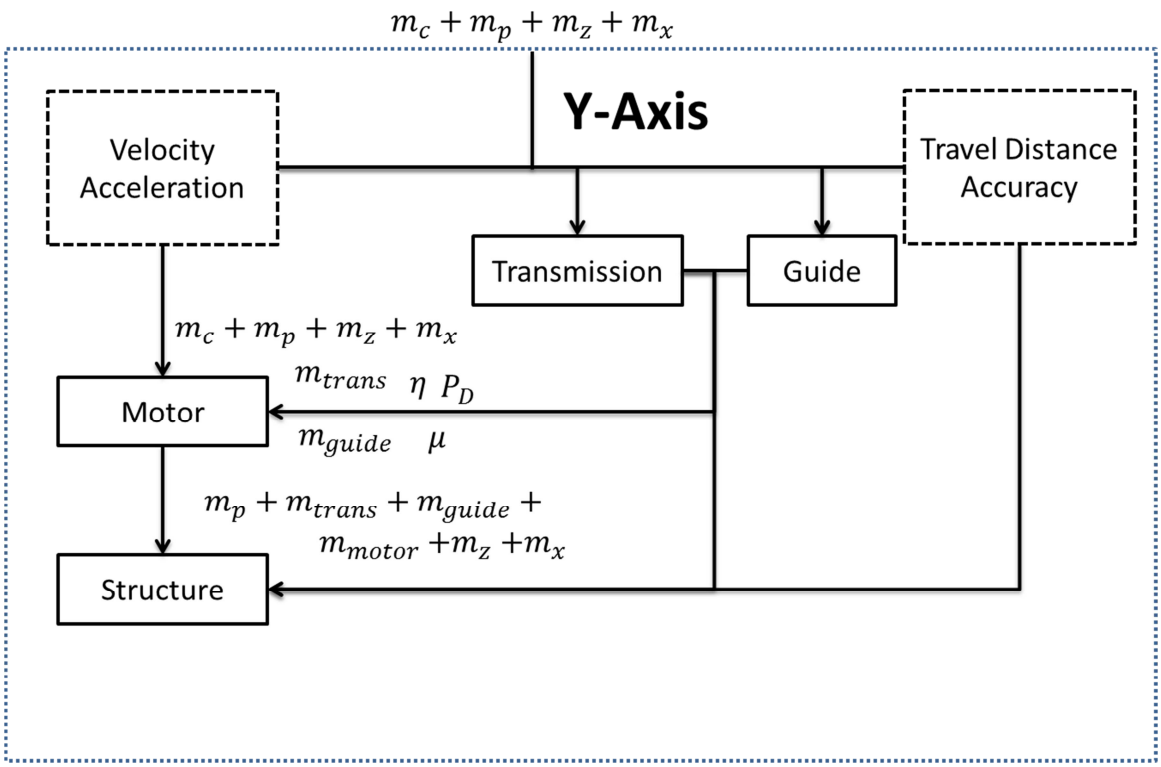

Figure 28: Y-axis Systems Diagram

5.3.4.1 Design Requirements

The design requirements for the y-axis are identical to the x-axis, except that the y-axis would have to support more weight. A travel distance of 244 in, accuracy of 0.74 inch, linear velocity of 97 ipm and an acceleration rate of 130.68 in/s^2 are desired for the y-axis as well. The systems has to support a weight of 23.43 lbs, half of the weight of the combined imaging system, pointing mechanism, z-axis, and x-axis since there are two members of the y-axis. Equation (5.35) shows that the y-axis must support a dynamic load of 31.36 lbs on each of the two sides of the y-axis.

$$F_{D\_y} = \frac{23.43\ lb}{32.2 ft/s^2} * 10.89 \frac{ft}{s^2} + 23.43\ lb = 31.36\ lb \qquad (5.35)$$

5.3.4.2 Guide and Transmission System

The same guide and transmission system is used on the y-axis as the x-axis since the design requirements are identical to the x-axis. Both the guide and transmission support a dynamic load it supports is greater than 31.36 lbs.

5.3.4.3 Motor

The motor on the y-axis has to actuate a total weight of 23.43 lbs. The motor should provide a linear velocity of 97 ipm, acceleration rate of 10.89 ft/s^2. Equation (5.36) shows that the motor needs to provide 9.12 oz-in of torque to actuate the object, with an 80 % factor of safety, a 0.04 inch equivalent pitch diameter, 80 % efficiency for the transmission system, and 88 % efficiency for the gear reduction mechanism.

$$\begin{aligned} \tau_{total} = \frac{0.04}{2(0.8)(0.8)(0.88)} \big(&0.014(23.43) \\ &+ 23.43/32.2\ ft/s^2(11\ ft/s^2)\big)\left(16\frac{oz}{lb}\right) \\ &= 9.12\ oz - in \end{aligned} \qquad (5.36)$$

Equation (5.37) shows that the motor must have a rotational velocity of at least 772 rpm at the desired torque to provide the desired linear velocity of the x and y-axis.

$$N = \frac{97}{0.04\pi} = 772\ rpm \qquad (5.37)$$

Any stepper motor that provides at least 9.12 oz-in of torque at 772 rpm will work for the x-axis. One of the stepper motors that meets this specifications is the Anaheim

Automation 11Y202 stepper motor, which provides approximately 9.2 oz-in of torque at 772 rpm, as shown in Figure 29. This motor has a weight of 0.18 lbs.

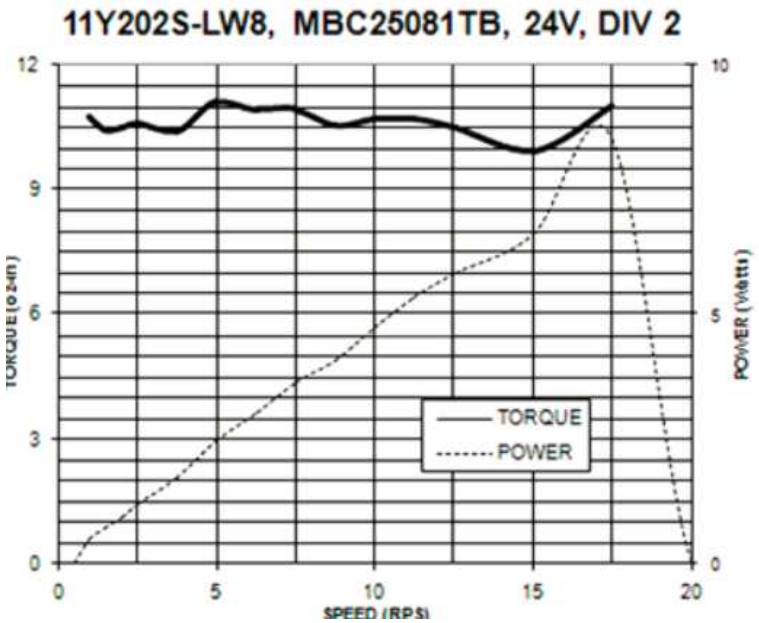

Figure 29: Anaheim Automation 08Y302 Torque Curve

5.3.4.4 Structure

The structure is required to support a weight of 46.75 lbs with a deflection that is less than 0.3 inch. The guide and transmission system for the y-axis has a weight of 23.14 lbs, the motor for the y-axis has a weight of 0.18 lbs, and the weight of the payload is 23.43 pound. Since the x-axis has a deflection of 0.44 in, the y-axis must deflect a maximum of 0.3 inch for the deflection in the z-axis to be less than 0.74 inch. Table 13 shows that a Model 1030 rail would meet the design constraints without additional reinforcements.

Table 13: Y-axis structure Selection

Model	Ix (in^4)	Iy (in^4)	A (in^2)	Weight (Lb/Ft)	Length (in)	weight (lb)	E (PSI)	Force (lb)	D (in)
1010	0.0442	0.0442	0.4379	0.5097	242	10.28	1E+08	46.75	3.735
1020	0.08333	0.3078	0.7914	0.9212	242	18.58	1E+08	46.75	0.614
1030	0.1238	0.9711	1.1596	1.3498	242	27.22	1E+08	46.75	0.220
2020	0.5509	0.5509	1.2079	1.406	242	28.35	1E+08	46.75	0.395
2040	1.0513	3.5168	2.2462	2.6146	242	52.73	1E+08	46.75	0.082
1515	0.2542	0.2542	1.154	1.3433	242	27.09	1E+08	46.75	0.841
1530	0.4824	1.8042	2.0798	2.4209	242	48.82	1E+08	46.75	0.153
3030	3.4133	3.4133	3.4477	4.0131	242	80.93	1E+08	46.75	0.108
3060	6.5164	22.03	6.4262	7.4801	242	150.85	1E+08	46.75	0.026

5.4 Design Summary

The motion mechanism design summery, shown in Table 14, suggests an AVT F-320 camera with an Edmund Optics NT67-709. However, any imaging system that supports an c-mount lens, has a 2080x1540 sensor resolution, 1/1.8 sensor size, and uses a 6 mm c-mount lens would not alter the design constraints for the positioning system provided that the imaging system weighs under one pound.

The motion mechanism is designed to have a travel distance of 242 in in the x-and y-axis and 17.31 distance in the z-axis, have a linear velocity of 97 in/min, and linear acceleration of 130.68 in/s^2. The system's accuracy requirement is +/- 0.37 inch from the center of the plant to prevent from the image from becoming out of focus and +/- 8.8 inch in the horizontal direction and +/- 3.4 in from the vertical direction for the image not to be cropped. These requirements were satisfied in the design of the positioning system.

Table 14: Motion Mechanism Design Summary

	Imaging System
Camera	AVT F-320
Lens	Edmund Optics NT67-709
	Pointing Mechanism
Model	Servo City DDT500
	Z-axis
Model	Parker LP28
	X-axis
Guide	Bishop Wisecarver W1SSX V-Groove
Transmission	Boston Gear 0.375 Face Width, 20 Pitch, 1.6 inch Pitch diameter Gear
Motor	Anaheim Automation 08Y202 Stepper
Gear Reducer	Thomson Linear NT23-030
Structure	80/20 Model 1020
	Y-axis
Guide	Bishop Wisecarver W1SSX V-Groove
Transmission	Boston Gear 0.375 Face Width, 20 Pitch, 1.6 inch Pitch diameter Gear
Motor	Anaheim Automation 11Y202 Stepper
Gear Reducer	Thomson Linear NT23-030

5.5 Positioning Mechanism System Limitations

While the proposed motion mechanism will satisfy the design requirements, it is important to understand possible constraints of this system. The work area of a fixed-position robotic system is the critical limiting factor in the motion system since it is governed by the length of the structural components. The structural components increase in weight as length increases, which require larger motors to actuate the structure. The increased length would also contribute significantly to the structural deflection since there is a cubic relationship between length and deflection. The increased work area

would also require a faster linear velocity to inspect a larger area in the allotted timeframe. The motor's maximum rotational velocity is another system limitation. A transmission system that contains a low gear ratio will increase system resolution, but will limit the system's maximum velocity.

CHAPTER 6

CONCLUSION

The goal of this thesis is to conduct the preliminary analysis for developing a plant inspection robot that is capable of providing the grower with multiple vantage points to visually plants. This thesis showed that the construction of this plant inspection robot is technologically feasible and can be built with commercially-available components, which would minimize development time and cost. Illumination and structural deflection were identified as the key design aspects to the design of the plant inspection robot.

Research highlighted in the literature review revealed that various plant stresses can be detected before visual symptoms appear and that robotic systems have been successfully developed and field-tested for complex applications such as selective-spraying. A Cartesian fixed-based motion system was identified as the most suitable platform for the plant inspection robot.

The design analysis showed that the plant inspection robot consists of an imaging system, which is responsible for image acquisition, and a motion mechanism, which is responsible for actuating the imaging system. The motion mechanism design is dependent on the design of the imaging system.

6.1 Imaging System Design

The imaging system design revealed that the vision system parameters were governed by illumination, shape, and size of the object along with the desired detail. The illumination was the critical parameter in the successful design of the vision system. Compromises must be made to maximize image quality if the illumination is insufficient. Increased sensor sensitivity, slower shutter speed, and larger aperture opening can all be used to compensate for the lack of illumination. However, the image will have less image

detail with higher sensor sensitivity, is more likely to experience motion blur with a slower shutter speed, and is more likely to be out of focus with a larger aperture opening.

6.2 Motion Mechanism Design

The motion mechanism design revealed that velocity, acceleration, work area, and accuracy govern its design. The system accuracy was defined by the depth of field, object size, and field of view of the imaging system. The z-axis travel distance was determined by the camera distance. The gantry-type structure required that the each sub-system to be designed successively, starting with the pointing mechanism, continuing with the z-axis, x-axis, and y-axis since the weight of each sub-system must be accounted when designing the subsequent sub-system.

The motion mechanism placed a great emphasis on the deflection of the x-axis in the z-direction since it could be only supported at the ends, whereas the z-axis was axially loaded, which would result in minimum deflection and the y-axis could be reinforced. The velocity and structural deflection would be more critical with a larger work area since a faster velocity is required to inspect more plants in the same timeframe and structural deflection because of the cubic relationship between structure length and deflection. The increased length would also increase the weight of the structural member itself and the weight of motion system components, which would further contribute to the deflection of the structure. Larger working areas would require heavier frames to resist deflection, requiring transmission systems that are sturdier and larger motors to actuate the structure. The torque curve of the motor must be accounted for when selecting the appropriate motor because of the inverse relationship between rotational velocity and motor torque.

6.3 Future Work

Future work could take the form of various different directions including motion system design and vision system design. Before these areas are explored, however, an

experimental setup must be constructed based on the analysis conducted to explore the practical feasibility of such a system and examine the design aspects that were unaccounted for in the system design analysis.

Imaging system under LED grow lights will have to be investigated since LED grow lights have become popular in recent years since it consumes a fraction of power compared to conventional artificial lighting sources without adverse effects on plant growth. However, LED-based artificial lighting system typically does not contain the color green since it is not critical to photosynthesis. The absence of the color green, however, will cause the plant leaves to appear to be gray.

Eventually, early detection methods should be integrated with visual inspection since the two methods complement each other. Early detection methods enable common plant stresses to be identified before visual symptoms appear while visual inspection enables a broader range of plant stresses to be detected. Research must be conducted on techniques that could be used to integrate these two inspection methods effectively and how to best display and use the information.

Future research in motion mechanism design can focus on development of multi-functional platform that would simultaneously utilize the imaging system for plant inspection and for machine guidance to perform a secondary function, such as precision spraying. Unconventional motion mechanisms that are still mostly in the research phases, such as cable-guided robots, should be further explored since some of these mechanisms may be better suited for the relatively low payload capacity and accuracy requirements for plant inspection.

BIBLIOGRAPHY

ACME Screw Assemblies. (2006). Retrieved March 12, 2012, from Nook Industries: http://www.nookindustries.com/acme/AcmeHome.cfm

Alaya-Silva, T., & Beyl, C. (2005). Changes in spectral reflectance of wheat leaves in response to specific macronutrient deficiency. *Advances in Space Research, 35*, 305-317.

Allen, E., & Triantaphillidou, S. (2011). *The Manual of Photography 10th Edition.* Oxford: Focal Press.

Astrand, B., & Baeveldt, A. (2002). An Agricultural Mobile Robot with Vision-Based Perception for Mechanical Weed Control. *Autonomous Robots, 13*(1), 21-35.

AVT Oscar Firewire.A Cameras. (2012). Retrieved March 9, 2012, from Edmund Optics: http://www.edmundoptics.com/products/displayproduct.cfm?productid=2871

Avery, D. (2007). How High-Yield Farming Saves Nature. *Social Science and Public Policy, 44*(6), 137-143.

Bakker, T., Asselt van, K., Bontsema, J., Muller, J., & Straten van, G. (2010). Systematic design of an autonomous platform for robotic weeding. *Journal of Terramechanics, 47*(2), 63-73.

Belforte, G., Deboli, R., Gay, P., Piccarolo, P., & Ricauda Aimonino, D. (2006). Robot Design and Testing for Greenhouse Applications. *Biosystems Engineering, 95*(3), 309-321.

Belforte, G., Gay, P., & Ricauda Aimonino, D. (2007). Robotics for Improving Quality, Safety and Productivity in Intense Agriculture: Challenges and Opportunities. *Advanced Robotic Systems.* Vienna, Austria.

Bishop Wisercarver DualVee Catalog. (2010). Retrieved 2 15, 2012, from Bishop Wisercarver: http://www.bwc.com/pdf/catalog/DualVee_Catalog_2010.pdf

Bock, C., Poole, G., Parker, P., & Gottawald, T. (2010). Plant Disease Severity Estimated Visually, by Digital Photography and Image Analysis, and by Hyperspectral Imaging. *Critical Reviews in Plant Sciences, 29*(2), 59-107.

Boston Gear Power Transmission Parts. (2012). Retrieved 2 17, 2012, from Grainger Industrial Supply: http://www.grainger.com/Grainger/boston-gear/ecatalog/N-1z12uic/Ntt-bases

Budynas, R., & Nisbett, J. (2011). *Shingley's Mechanical Engineering Design.* New York, NY: McGrall Hill.

Bulanon, D., Kataoka, T., Ota, Y., & Hiroma, T. (2002). A Segmentation Algorithm for the Automatic Recognition of Fuji Apples at Harvest. *Biosystems Engineering, 83*(4), 405-412.

Burks, T., Shearer, S., & Donohue, K. (2000). Backpropagation Neural Network Design and Evaluation for Classifying Weed Species Using Color Image Texture. *Transactions of the ASAE, 43*(4), 1029-1037.

Burks, T., Villegas, F., Hannan, M., Flood, S., Sivaraman, B., Subramanian, V., et al. (2005). Engineering and horticultural aspects of robotic fruit harvesting: Opportunities and constraints. *HortTechnology, 15*(1), 79-87.

Chaerle, L., Hagenbeek, D., De Bruyne, E., Valcke, R., & Van Der Straeten, D. (2004). Thermal and Chlorophyll-Fluorescence Imaging Distinguish Plant-Pathogen Interactions at an Early Stage. *Plant Cell Physiology, 45*(7), 887-896.

Critten, D., & Bailey, B. (2002). A review of greenhouse engineering developments during the 1990s. *Agricultural and Forest Meteorology, 112*, 1-22.

Compact Fixed Focal Length Lenses. (2012). Retrieved March 9, 2012, from Edmund Optics: http://www.edmundoptics.com/products/displayproduct.cfm?productid=3070

Figliola, R., & Beasley, D. (2006). *Theory and Design for Mechanical Measurements.* Hobokey: John Wiley & Sons.

Finch, G. (2011). *Photographing Children Photo Workshop, 2nd Edition.* Indianapolis: Wiley.

Fjallman, T., & Hall, J. (2005). Antibody engineering- a valuable asset in preventing closed environment epidemics. *ACTA Astronautica, 57*, 81-88.

Foglia, M., & Reina, G. (2006). Agricultural Robot for Radicchio Harvesting. *Journal of Field Robotics, 23*(6-7), 363-377.

Folta, K., Koss, L., McMorrow, R., Kim, H., Kenitz, J., Wheeler, R., et al. (2005). Design and fabrication of adjustable red-green-blue LED light arrays for plant research. *BMC Plant Biology, 5*(17).

Freeman, M. (2008). *Pro Photographer's D-SLR Handbook.* Cambridge, England: Ilex.

Funakubo, H. (1991). *Actuators for control.* Amsterdam: OPA.

Gerlach, J., & Gerlach, B. (2010). *Digital Landscape Photography.* Burlington: Focal Press.

Giacomelli, G., Patterson, R., & Sadler, P. (2007). Telepresence Technologies and Practices for Enabling Remote Semi-Autonomous CEA Food Production. *Acta Hort (ISHS) 761*, 21-31.

Glacern Machine Tools. (2012). Retrieved March 15, 2012, from Glacern Machine Tools: http://www.glacern.com/sbr

Gonzalez, R., Rodriguez, F., Sanchez-Hermosilla, J., & Donaire, J. (2009). Navigation Techniques for Mobile Robots in Greenhouses. *Transactions of the ASABE, 25*(2), 153-165.

Gorbe, E., & Calatayud, A. (2010). Optimization of Nutrition in Soilless Systems: A Review. *Advances in Botanical Research, 53*, 193-245.

Groover, M. (2001). *Automation, Production Systems, and Computer-Integrated Manufacturing.* Upper Saddle River: Prentice Hall.

Harris, D. (1992). *Hydroponics: the complete guide to gardening without soil.* London: New Holland Publishing.

Hart, D. (1996). *The camera assistant: a complete professional handbook.* Newton: Butterworth-Heinemann.

Hayashi, S., Ganno, K., Ishii, Y., & Tanaka, I. (2002). Robotic Harvesting System for Eggplants. *JARQ, 36*(3), 163-168.

Hayashi, S., Shigematsu, K., & Yamamoto, S. (2010). Evaluation of a strawberry-harvesting robot in a field test. *Biosystems Engineering, 105*, 160-171.

Hornberg, A. (2006). *Handbook of Machine Vision.* KGaA, Weinheim: Wiley-VCH.

Jensen, M. (2002). Controlled Environment Agriculture in Deserts, Tropics and Temperate Regions- A World Review. *578*, 19-25.

Johnson, D., Naffin, D., Puhalla, J., Sanchez, J., & Wellington, C. (2009). Development and Implementation of a Team of Robotic Tractors for Autonomous Peat Moss Harvesting. *Journal of field Robotics, 26*(6-7), 549-571.

Jones, A. (2004). *The Step-By-Step Photography Workshop: More than 50 Illustrated Techniques for Improving Your Work.* Cincinnati: Writer's Digest Books.

Jones, B. (2005). *Hydroponics: a practical guide for soilless grower, Volume 1*. Boca Raton: CRC Press.

Kacira, M., Ling, P., & Short, T. (2002). Machine Vision Extracted Plant Movement for Early Detection of Plant Water Stress. *Transactions of the ASABE, 45*(4), 1147-1153.

Kassler, M. (2001). Agricultural Automation in the new Millennium. *Computers and electronics in agriculture, 30*, 237-240.

Kent, W. (1916). *The Mechanical Engineers' Pocket Book.* New York: John Wiley & Sons.

Kondo, N., & Ting, K. (1998). Robots for Plant Production. *Artificial Intelligence Review, 12*, 227-243.

Lamm, R., Slaughter, D., & Giles, D. (2002). Precision Weed Control System for Cotton. *Transactions of the ASABE, 45*(1), 231-238.

Lee, W., Slaughter, D., & Giles, D. (1999). Robotic Weed Control Systems for Tomatoes. *Precision Agriculture, 1*, 95-113.

Li, H., Xu, Z., & Tang, C. (2010). Effects of light-emitting diodes on growth and morphogenesis of upland cotton (Gossypium hirsutum L.) plantlets in vitro. *Plant Cell Tiss Organ Cult., 103*, 155-163.

Linear Units Quick Selection Guide. (2012). Retrieved March 1, 2012, from Thomson Linear Motion: http://www.thomsonlinear.com/website/com/eng/download/document/Linear_Units_Quick_Selection_Guide_bren.pdf

LS100 Series User's Guide. (n.d.). Retrieved 2 14, 2012, from Anaheim Automation: http://www.anaheimautomation.com/manuals/table/L010765%20-%20LS100%20Table%20Manual.pdf

McCarthy, C., Hancock, N., & Raine, S. (2010). Applied machine vision of plants - a review with implications for field deployment in automated farming operations. *Intelligent Service Robotics, 3*(4), 209-217.

Modern Linear. (2004). Retrieved March 12, 2012, from Modern Linear: http://www.modernlinear.com/

Okayama, T., Okamura, K., Park, J., Ushada, m., & Murase, H. (2008). A Simulation for Precision Airflow Control using Multi-Fan in a Plant Factory. *Environ. Control Biol., 46*(3), 183-194.

Overby, A. (2010). *CNC Machining Handbook.* New York: McGraw-Hill.

Pacific Bearing Company. (2012). Retrieved March 12, 2012, from Pacific Bearing Company: http://www.pbclinear.com/Profile-Rail-Technology---Ball-type-Linear-Guide-Rails

Planetary Gear Boxes Specifications. (2011). Retrieved 11 08, 2011, from Techno-Isel: http://www.techno-isel.com/tic/Catdas/PDF/Gearboxes.pdf

Phan, C., Brach, E., & Jasmin, J. (1979). STUDIES ON THE DETECTION OF LETTUCE MATURITY: ANATOMICAL OBSERVATIONS AND REFLECTANCE MEASUREMENTS IN THE VISIBLE RANGE. *Canadian Journal of Plant Science, 59*(4), 1067-1075.

Pilarski, T., Happold, M., Pangels, H., Ollis, M., Fitzpatrick, K., & Stentz, A. (2002). The Demeter System for Automated Harvesting. *Autonomous Robots, 13*(1), 9-20.

Sandini, G., Buemi, F., Massa, M., & Zucchini, M. (1990). Visually guided operations in greenhouse. *Proceedings of the IEEE International Workshop on intelligent Robots and Systems IROS '90*, 279-285.

Schmidt, P. (2011). *The Complete Guide to Greenhouse and Garden Projects.* Minneapolis: Creative Publishing International.

Shaw, J. (1994). *John Shaw's Landscape Photography.* New York: AMPHOTO.

Slaughter, D., Giles, D., & Downey, D. (2008). Autonomous robotic weed control system: A review. *Computers and Electronics in Agriculture, 61*, 63-78.

Slaughter, D., Giles, D., & Downey, D. (2008). Autonomous robotic weed control system: A review. *Computers and Electronics in Agriculture, 61*, 63-78.

Slaughter, D., Giles, D., Fennimore, S., & Smith, R. (2008). Multispectral Machine Vision Identification of Lettuce and Weed Seedlings for Automated Weed Control. *Weed Technology, 22*(2), 378-384.

Slaughter, D., Giles, D., Fennimore, S., & Smith, R. (2008). Multispectral Machine Vision Identification of Lettuce and Weed Seedlings for Automated Weed Control. *Weed Technology, 22*(2), 378-384.

SPT 200 Specification. (2012). Retrieved 2 15, 2012, from Servo City: http://servocity.com/html/spt200_pan___tilt_system.html

Story, D., Kacira, M., Kubota, C., Akoglu, A., & An, L. (2010). Letuce calcium deficiency detection with machine vision computed plant features in controlled environments. *Computers and Electronics in Agriculture, 74*, 238-243.

Techno Automation. (2012). Retrieved March 20, 2012, from Techno Automation: http://www.technoautomation.com/

Van Henten, E., & Bontsema, J. (1995). Non-destructive Crop Measurements by Image Processing for Crop Growth Control. *J. agric. Engng Res., 61*, 97-105.

von Wichert, G. (1998). Mobile Robot Localization Using a Self-organized Visual Environment Representation. *Robotics and Autonomous Systems, 25*(3-4), 185-194.

Woebbecke, D., Meyer, G., Von Bargen, K., & Mortensen, D. (1995). Shape Features for Identifying Young Weeds Using Image Analysis. *Transactions of the ASAE, 38*(1), 271-281.